AD-A117 543 STEVENS INST OF TECH HOBOKEN N J DEPT OF MECHANICAL --ETC F/G 1/3
RESEARCH ON THE BEHAVIOR OF CASCADED AIRFOILS UNDER CONDITIONS --ETC(U)
JUN 82 N00014-79-C-0765

UNCLASSIFIED NL

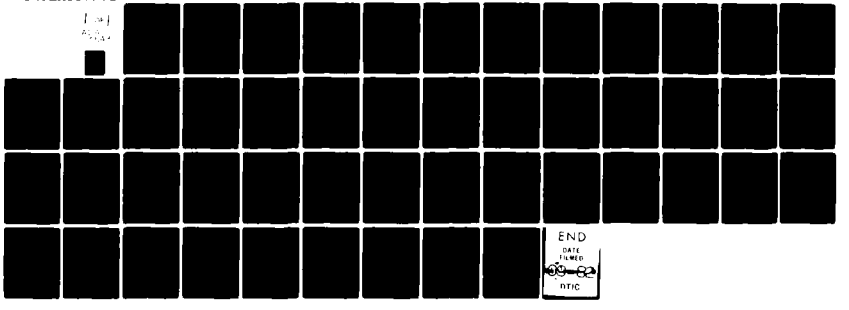

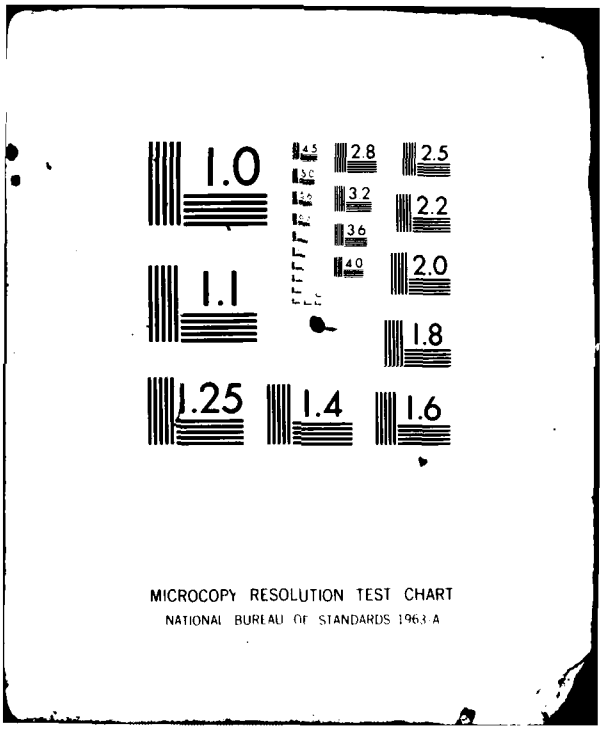
1.0
1.1
1.25
1.4
1.6
1.8
2.0
2.2
2.5
2.8
3.2
3.6
4.0
MICROCOPY RESOLUTION TEST CHART
NATIONAL BUREAU OF STANDARDS 1963-A

(12)

FINAL TECHNICAL REPORT

TO

OFFICE OF NAVAL RESEARCH
Project SQUID

ON

Contract No. N00014-79-C-0765 NR-094-391

Entitled

RESEARCH ON THE BEHAVIOR OF CASCADED AIRFOILS UNDER CONDITIONS OF HIGH MEAN LOADING AND FLOW UNSTEADINESS

15 September 1979 to 31 January 1982

F. Sisto
Professor Mechanical Engineering
Project Manager

Mechanical Engineering Department
Stevens Institute of Technology
Hoboken, New Jersey 07030

30 June 1982

SUMMARY

This contract, transferred to the auspices of the SQUID program effective 1 March 1981, was originally planned as a three year program.

The objectives were predominantly experimental in nature: to measure the unsteady velocities in the rotor passage of a single stage axial flow compressor and map the velocity field at operating conditions near rotor blade stall. For this purpose a laser doppler velocimeter was to be developed and married to a new single stage axial flow compressor designed expressly for this purpose.

At the premature conclusion of the contract, the first successful velocity determination in the running compressor had not been obtained, although the LDA and its associated subsystem was operational.

Some compressor cascade modelling studies, ultimately intended to be guided, or "calibrated" by the experimental results are only partially completed.

DISCUSSION

The single stage compressor was constructed under this contract and a variable speed control procured for setting the compressor operating point in conjunction with a discharge throttle valve. This system is running satisfactorily and the present status may be described as being in the midst of modifications to: a) improve the optical quality of the laser beam penetration and return through the transparent housing, b) mount the LDA on an adjustable frame to permit an accurate determination and viewer adjustment of the measuring

volume location in 3-space and c) procure and install of a set of exit guide vanes to provide more realistic compressor loading characteristics in later tests. The last item is being pursued as part of a master's thesis and it is not essential for the first series of anticipated tests.

In conjunction with these physical modifications a parallel development of the LDA data acquisition and processing circuitry is in final stages of micropressor development involving breadboarding etc. Studies directed toward processing the data in its anticipated "sparse" form are being conducted by Dr. Cole and his graduate (and undergraduate) students. This work is described and recorded in greater detail in Appendix A to this report.

Modelling studies of a preliminary nature have been completed for the particular high loading/unsteady flow phenomenon described as "propagating stall". A very simple case of unstaggered, uncambered thin airfoils has been analyzed for nonuniform distribution of loading from blade to blade in a two-dimensional cascade. This work is detailed in Appendix B to this report. The principal value of this latter study are the demonstration of the possibility of lift-distribution anomalies and as a clear guide to the inclusion in the model of downstream shed vorticity and stability considerations which do not appear in the work shown in that appendix.

Personnel who have been supported under the terminated contract include, in addition to the Project Manager and the Principal Investigator, the following graduate (G) and undergraduate (U) students (the latter being assigned exclusively to apparatus construction and

computing):

Yao Andrew Tang (G)	David Sharp (U)
Richard Feltman (G)	Raymond Johnson (U)
Kenneth Bird (U)	Tom Hughes (G)
Stephen Olson (U)	Fady Khairallah (U)

Stemming from the nature of the work (design and procurement of an experimental apparatus) it was not appropriate to assign academic thesis credit to the graduate students for their contributions; it is anticipated that future work on this subject will involve both analytical and experimental phases and will be suitable masters thesis and doctoral dissertation material. The elucidation of unsteady flow phenomena at high blade loading remains a fundamental topic of great importance in designing and operating axial flow compressors.

CONCLUSIONS

With respect to data-reduction methods for the subject LDA measurements, several conclusions can be drawn. From an extensive literature search and review, along with professional consultations, it is concluded that the theoretical extensions by Papoulis and by Yen are apparently the only existing basis for dealing with the unusually "sparse" data of the gated-LDA situation. Through these extensions or adaptations of them, it is theoretically possible to determine unsteady velocities via sparse bursts of samples randomly spaced within bursts. From numerical simulations, Papoulis' "bunched-sample" approach is concluded to be satisfactorily insensitive to most parametric influences on the data-reduction process (random error, time spacing of samples, number of samples, etc.). However,

the possibility of high sensitivity to missing data samples warrants further study before this approach can be reasonably assured of viability. Preliminary investigation of Yen's "migrated-sample" approach however, suggests that this approach may not be satisfactory though not conclusively. It is concluded that a third alternative justifies further study via simulation - Yen's "minimum-energy" approach. It is finally concluded that, at least until one or more of these approaches can be more definitively found satisfactory, it is appropriate to make LDA measurements in successive blade passages, interpreting such values using reasonable, if not provable, a priori assumptions concerning the nature of unsteady velocities in neighboring blade passages.

With respect to analytical/computer modelling of stall "cells" at high cascade loading conditions, a beginning study has shown that, for a one-blade cell, boundary conditions may be satisfied on all blades (stalled and unstalled). The solution exhibits local regions of reverse flow. It appears to be perfectly straightforward to extend the method to multiblade cells in cascades with both camber and stagger; it is expected that a richer variety of individual blade loadings, within and without the cell, will be exhibited by this solution. The features which are lacking, and which should be incorporated in the model, in any future work, are a recognition of time dependence and consequently the induction effects of the shed vorticity downstream of the cascade. With the successful inclusion of these two key effects in the model it should be capable of predicting the unsteady (vector) velocity at a fixed point in the cascade flow and hence the quantities to be measured by the LDA.

APPENDIX A

GATED DIGITAL SAMPLING FOR TURBOMACHINES

I. INTRODUCTION

The prospect of LDA measurements of in-rotor air velocities in a test turbocompressor leads inherently to concern in the area of digital data processing. This Appendix reports results of a search for potentially useful theoretical treatments and also subsequent numerical simulations based on such theory. Simulations are particularly necessary because of the unconventional situation presented by LDA measurements of in-rotor velocities. The desire to measure unsteady in-rotor velocities presents a data-processing situation apparently undeveloped heretofore.

A computer-aided literature search uncovered useful existing theories and applications of pertinent digital signal analysis. Because of the inherent randomness and the sparseness of data sampling which was expected from the LDA/turbo-compressor measurements, particular emphasis was given in the literature search to irregular or non-uniform spacing of samples in time. Engineering Index and National Technical Information Service data bases were searched resulting in a variety of useful references. Over 30 references were reviewed as a result, and based on them, further secondary references were uncovered. In addition, electrical engineering and mathematics faculty who are experienced in digital sampling matters were consulted. This and the literature search led to the conclusion that the subject situation was not dealt with effectively by existing developments. A review of the conditions of conventional digital sampling theory makes clear the distinctive features

encountered in the subject LDA application.

It is well-established in the theory of digital signal analysis ("sampling theorem", Whittaker, 1915; Shannon, 1949) that an infinite set of instantaneously-taken samples from such a signal contains all the information, i.e., complete specification, of the original signal, f(t), if the signal is bandwidth-limited, i.e., if its frequency components do not exceed a limiting value (Stearns, 1975). In fact, the signal can be exactly reconstructed from its sampled values by appropriately weighting contributions from all the sample values:

$$f(t) = \sum_{n=-\infty}^{\infty} f(t_n) \frac{\sin[\pi f_s(t-t_n)}{\pi f_s(t-t_n)} \qquad \text{(A-1)}$$

where: t_n is the time of the nth sample

f_s is the frequency of sampling

This is strictly true if f(t) is limited to frequency components less than 1/2 f_s but only approximately true otherwise. For a given bandwidth - limited signal, then, the sampling frequency must exceed twice the highest signal frequency. This minimum sampling frequency is sometimes termed the "Nyquist frequency".

From one point of view, the need for limiting the bandwidth of f(t) can be thought of as a necessity in order to avoid "aliasing", i.e., the erroneous interpretation of high-frequency periodicity as if it derived from signal components at low frequency. Such incorrect interpretation is familiar hazard of using a stroboscope to determine rotational speed.

A second source of error in the practical use of the sampling theorem arises from the need to deal with a finite set of samples. In practice, "truncation" of the theoretically infinite series representing f(t) leads to so-called "truncation error" which is unavoidable.

Unfortunately, however, velocities measured by an LDA cannot be thought of as even a finite number of the equally-spaced samples deal with in conventional sampling theory.

II. DIGITAL SAMPLING IN LDA MEASUREMENTS

The concept of laser doppler anemometry has several alternative implementations, the most common method can be visualized as small particles (traveling with a fluid flow) traversing a "measuring volume" in space in which crossed laser beams produce a constructive/destructive optical interference pattern. As particles pass from light to dark regions of the interference "fringe" pattern within the measuring volume, more or less light is scattered and eventually received by a photodetector. This results in a time-wise modulation of the photodetector output signal related to the speed of the scattering particle. The time at which such a particle enters the measuring volume is essentially random. Therefore, the velocity value determinable from the modulated photodetector signal must be considered as representative of a randomly selected time. Successive determinations are, therefore, not at the equal time spacing dealt with by the sampling theorem for digital signals but rather at random time spacing.

Despite the inherently-random times at which such LDA measurements are made, it is conceivable to establish corresponding

equally-spaced sample values to which the sampling theorem and corresponding data-reduction methods (e.g., Fast Fourier Transform) could apply. This might be accomplished by fitting appropriate smoothed curves to the randomly timed data samples (as an approximation to the original continuous function representing time-varying velocities). These smoothed approximations might then be resampled at equally spaced intervals to yield the requisite sets of equally-spaced sample values which admit conventional data reduction.

Beside resampling in order to give equally-spaced samples, it is even theoretically possible to deal with original randomly-spaced sample values themselves; the sampling theorem can be extended to randomly-spaced samples, and the sufficiency of an (infinite) number of such samples for determining signal spectra or even reconstructing signal functions is assured (Loo, 1969). Thus, if randomness of sample spacing were the only complication of the subject LDA/turbocompressor measurements, random-sampling extensions of conventional theory would be available and applicable. Unfortunately, in-rotor LDA measurements require "gating" of the usual (randomly-spaced) LDA measurements, i.e., accepting only those measured values occuring within well-defined time periods as is discussed in the next section.

III. GATED DIGITAL SAMPLING

Measurements of gas velocities in turbomachine rotors have been accomplished by various workers who have determined mean and sometimes root-mean-square velocities from "gated" LDA measurements. This approach requires the accepting of data only if it is measured during a brief time period (gate "open") when one small region within one blade passage falls within the measuring volume of the LDA.

Figure A-1 illustrates this scheme. Successive measurements taken from successive revolutions of the rotor have been time-averaged by some researchers and r-m-s values calculated in order to "map" mean gas velocities and their variances or deviations within rotor blade passages. To move beyond mean and r-m-s velocity determinations into unsteady, time-resolved measurements forces confrontation with the sampling theorem and its ramifications.

If only (as shown in Fig. A-1) a single velocity value is measured during each gating period (once per rotor revolution), the sampling theorem clearly restricts the obtainable information to signal components of frequency less half the rotor speed (half the Nyquist frequency). Components at such low frequencies are not of greatest interest aerodynamically. The question immediately arises as to whether it is possible from gated LDA measurements to provide information concerning higher frequency components of the unsteady gas velocities.

Fortunately, an old "folk theorem" of digital sampling theory was uncovered. This states that a "signal f(t) may be represented by anylinear combination of <u>irregularly</u> spaced samples $f(t_n)$, provided the <u>average</u> sampling rate exceeds the Nyquist rate, i.e., that the number of samples per unit of time exceed (on the average) twice the highest frequency present in the signal (Beutler, 1966). Beutler has, in fact, shown that "only the past need be sampled at an average rate greater than the Nyquist rate to assure error-free recovery". In this context, <u>multiple</u> LDA measurements during short once-per-revolution gating periods can theoretically provide the means for deriving measurements of unsteady velocity components at frequencies even exceeding the rotational frequency of a turbomachine rotor.

However, the mathematical theory assuring the possibility of LDA measurements of unsteady velocity is separate from the question of how to do this i.e., a practical data-reduction scheme. Unfortunately, the literature seems to be devoid of a data-reduction algorithm or approach matched to the gated LDA situation. This forced investigation of approaches available for similar, if not identical, data-reduction tasks as described in the next section.

IV. AVAILABLE THEORY

Two available approaches to digital sampling provide extensions to conventional theory which are distinctly applicable to the subject gated-LDA measurements. Other authors have established the sufficiency of samples spaced randomly in time (e.g., Loo, 1969) and the significance of the average sampling rate as the equivalent (for non-uniform sample spacing) of the Nyquist-limit sampling rate (for equally-spaced samples) (Beutler, 1966). However, it appears that only the two works cited following provide expressions for actually carrying out the theoretically-justified reconstruction based on non-uniformly-spaced sample data.

First, Papoulis (1977) has generalized the specifications for sample sets from which a signal can be reconstructed to allow for the possibility of non-uniform sample spacing. Papoulis' formulation provides for "bunching" of samples, i.e., a non-uniform sample spacing within a finite-sized "bunch" of samples with unending recurrence of the same non-uniform, in-bunch spacing over successive bunches (see Fig. A-2). Reconstruction of the original signal, f(t), from sample values is, in general:

$$f(t) = \sum_{n=-\infty}^{\infty} g_i(nT)y_1(t-nT) + g_2(nT)y_2(t-nT)t \ldots + g_n(nT)y_n(t-nT) \quad \text{(A-2)}$$

where: T is the period of recurrence of bunches

n is the running index designating a specific bunch (of non-uniformly-spaced samples)

m is the running index designating a specific sample (within a single bunch and recurring within successive bunches)

g_m is a function defining the samples values as a function of time

y_m is the reconstruction function for all samples at position "m" in all bunches.

Among other possibilities, Papoulis' theory includes provision for sample functions $g_i(t)$ which take the value of the signal at some well-defined time leading or lagging the sampling time (i.e., for arbitrarily time-dispersed sampling). Alternatively, the theory allows for sample functions which take the value of one or more derivatives of the signal function as well as the function itself at the sampling times.

Papoulis' formulation, then, allows generalization of the timing and definition of sample values but always within the context of recurring, repetitive sample bunches. Figure A-3 illustrates two examples of this generalization for which Papoulis developed specific reconstruction formulae. The second example, which involves bunching of samples in twos, can be seen to resemble gated-LDA sampling but with repeated regular sampling patterns rather than random patterns during successive gates.

A second potentially useful extension is that formulated by Yen (1956). Yen developed four specific extensions, one of which allows for the "migration" of a finite number of conventional, equally-spaced samples to arbitrary sampling times (see Fig. A-4).

For equally-spaced samples, reconstruction of limited-bandwidth signal functions f(t) from an infinite sample set $\{f(t_n)\}$ is accomplished (as described above) via (after Whittaker and Shannon):

$$f(t) = \sum_{n=-\infty}^{\infty} f(t_n) \frac{\sin[\pi(t-t_n)/T_s]}{\pi(t-t_n)/T_s} \qquad \text{(A-3)}$$

where: T_s is the (fixed) time period between successive samples. Equally-spaced samples are seen to result in the same weighting or reconstruction function $(\sin(\pi(t-t_n)/T_s)/\pi(t-t_n)/T_s)$ for each individual sample value, $f(t_n)$.

As an extension for non-uniformly-spaced samples, Yen considers a different weighting or reconstruction function for each different non-uniformly spaced sample, $f(t_p)$ (total of N values) and for each different time, t:

$$f(t) = \underbrace{\sum_{p=1}^{N} f(t_p)\ \Psi_p(t)}_{\text{non-uniformly-spaced samples}} + \underbrace{\sum_{\substack{q=-\infty \\ \neq p}}^{\infty} f(t_q)\ \Psi_q(t)}_{\text{remaining uniformly-spaced samples}} \qquad \text{(A-4)}$$

Yen derives general expressions for the (different) Ψ_p and Ψ_q functions.

Another of Yen's extensions deals with a finite number of arbitrarily-spaced samples used to reconstruct the original signal. This allows unique solution if the resulting, reconstructed sample

function is constrained to minimize its "energy" (integral of its amplitude squared).

Both of Yen's and Papoulis' extensions are significantly close to the subject LDA situation to allow dealing with gated LDA measurements. Papoulis' recurrent spacing pattern could be imposed by smoothing the original, randomly spaced LDA sample values from the LDA and resampling (interpolating) to gain the necessary recurrent pattern of sampling times.

However, both Papoulis' and Yen's theories apply rigorously only for an infinite number of samples (just as does the Whittaker reconstruction algorithm for equally-spaced samples). Neither addresses the question of errors introduced by the truncation to finite-size data sets as required in practice. A further necessary concern for error which is lacking in Papoulis' and Yen's treatments relates to the specific sort of bunching of data anticipated in the gated LDA sutiation - sparse data occurring in bursts with relatively long data-free interludes between bursts. No treatment of such practically crucial concerns was found in the literature. Therefore, computer simulations were carried out to provide insight into the practicality of applying Papoulis' or Yen's extensions to the subject LDA experiments. These are described in the following section.

A. RECURRENT BUNCHED SAMPLES

The sampling-theory generalization by Papoulis (1977) is particularly easily formulated for the specific case of two data samples per bunch. This case is given as an example by Papoulis. While LDA experiments give non-recurrent, random data spacing within

bunches, such data could be converted to samples satisfying Papoulis' example-scheme by data smoothing and resampling. A computer simulation was programmed in order to evaluate parametric influences on the accuracy of signal reconstruction and subsequent spectral analysis according to Papoulis' scheme.

A.1 INFLUENCE OF RELATIVE FREQUENCY OF SIGNAL & SAMPLING

Several simulation runs were made with sample sets of 6 pairs (bunches) of samples taken from a pure sine wave. To approximate the sparse data of the grated LDA situation the time interval between the paired sample of each "bunch" was 0.02 units on a scale of 1 time unit between bunches (see Fig. A-5). Figure A-6 shows the original (sinusoidal) signal and the pairs of sample points superimposed for a case in which the signal frequency is 0.9 of the frequency at which bunches of samples are taken. The frequency of occurrence of bunched samples corresponds with the gating frequency for gated-LDA measurement (or the turbomachine rotational speed in the subject experiments). For the purpose of these and further plots, times are non-dimensionalized by the period between gates (period of turbomachine rotation).

Figure A-7 shows a reconstruction of the signal of Figure A-6. The reconstruction is based on the (bunched) sample points (which are shown) and on Papoulis' reconstruction equation:

$$f(t) = \frac{\cos\frac{2\pi}{T}\alpha - \cos\frac{2\pi}{T}t}{\frac{2\pi}{T}\sin\frac{2\pi}{T}\alpha} \sum_{n=-\infty}^{\infty} \left[\frac{f(nT+\alpha)}{t-nT-\alpha} - \frac{f(nT-\alpha)}{t-nT+\alpha}\right] \qquad \text{(A-5)}$$

where f(t) is the signal function

2α is the (non-dimensional) time interval between paired samples (within a burst)

T is the (nominal) sampling period (time between sample bunches)

n is the running index designating different bunches

The figure illustrates the occurrence of "leakage", i.e., non-zero values (oscillations) of the reconstructed signal outside the time span of the original sampling (approx. t = 0 to t = 5). The figure also shows that reasonably faithful reconstruction is feasible even when the signal frequency (0.9 in Figs. A-6 and A-7) is close to the nominal bunched-sample frequency (1.0). Similar results are shown in Figure A-8 for which the relative phase of the signal and the bunched sampling is varied, maintaining the same frequencies as in Figures A-6 and A-7.

Successively increasing the signal frequency to well above the nominal sampling frequency shows, first, increased distortion and finally gross error in the reconstructed signal. This trend reflects the theoretical limitation of the reconstruction process (even using an infinite sample set) to signal frequencies less than one-half the time-averaged sampling frequency. In this case, the time-averaged sampling frequency is (2 samples per bunch) x (1 time unit per bunch) = 2 samples per time unit. Therefore, the signal frequency should not exceed 1.0 cycle per time unit. In fact, the reconstruction of signals of frequencies 1.1 and 1.3 cycles per unit time (Fig. A-9) is seriously in error.

A.2 INFLUENCE OF SAMPLE MEASUREMENT ERRORS

The effect of random experimental errors in measuring sample values was also simulated. Random errors were added (or subtracted) to the calculated (sinusoidal-signal) sample values which were previously used. The random errors were taken to have zero mean value and an arbitrarily specified standard deviation. Fig. A-10 illustrates the increasing degradation of the reconstructed signal in terms of reconstructed signal shape as the standard deviation of experimental error increases. At least for the baseline conditions of this simulation (12 sample points, signal freq. = 0.9 max. allowable signal freq., Figs. A-6 and A-7), random error with standard deviation exceeding several percent is clearly unacceptable. Even doubling the number of samples does not seem to alter such a conclusion much (Fig. A-11) as is especially evident in the resulting power spectra (Fig. A-12).

A.3 INFLUENCE OF NUMBER OF SAMPLES (SAMPLING DURATION

Simulations for varying numbers of bunches of paired samples were carried out. Fig. A-13 illustrates the results, with respect to shape of the reconstructed signal itself and Fig. A-14 shows the corresponding power spectra. Increased numbers of data are seen to improve spectral discrimination considerably as is expected, but the high spectral signal/background-noise (e.g., 7/1, Fig. A-14) for a modest number of samples (24) was unexpectedly encouraging.

A.4 INFLUENCE OF GATE DURATION

In the subject, gated-LDA situation, the "gate-open" interval is but a small fraction of the total experiment (sampling) interval,

for example, 0.001 to 0.01. Short "gate-open" intervals imply decreased probability of a valid LDA measurement during that interval but increased spatial resolution in measuring turbomachine rotor blade-passage velocities. Short gate-open intervals can also be expected to degrade the accuracy of reconstructing signals or gaining spectral data from samples taken during such short intervals. To help evaluate these effects, several simulations computer runs were made with varying time between the (paired) samples within a bunch or burst (2α in Eq. A-5).

Fig. A-15 and A-16 show how reconstructed-signal shapes and their spectra respond to increasing bunching of samples without change in average sampling rate. Clearly, very sparse samples, (i.e., widely separated bunches or "bursts") are feasible without severe degradation of signal-reconstruction possibilities using Papoulis' scheme.

B. FINITE SET OF NON-UNIFORMLY-SPACED SAMPLES (EMBEDDED IN INFINITE SET OF UNIFORMLY-SPACED SAMPLES)

The sampling-theory generalizations by Yen (1956) appear particularly applicable to the subject gated-LDA measurements. Unlike Papoulis' generalization, those of Yen allow arbitrarily-spaced samples, consistent with the gated LDA measurements which are expected to occur at random times within sparse bursts. Yen's approach has been demonstrated, on the other hand, to require relatively long computation times (Sankur and Gerhardt, 1973). This is not, however, a crucial shortcoming for the subject application.

Much more likely to be practically significant is the fact that Yen's reconstruction functions can be expected to assume large values between sample points. This leads to potential computational difficulties. The required summation of terms (Eq. A-4) seems necessarily to lead to calculating small differences between large numbers (from different terms) yielding potentially large errors. This potential problem as well as the problem of errors due to truncation to a finite number of samples has led to numerical computer simulation. Computer programming to allow this simulation is in progress but at this date has not yet been completed, and its results cannot be reported here. Preliminary results do, however, suggest strongly that the problems cited above are probably excessive rendering this alternative impractical.

C. NON-UNIFORMLY-SPACED SAMPLES AND "MINIMUM ENERGY" RECONSTRUCTION

This alternative approach to gated-LDA applications, while potentially promising, had not yet been programmed for computer simulation.

REFERENCES

1. Beutler, F.J., "Error-Free Recovery of Signals from Irregularly-Spaced Samples", S.I.A.M. Review, 8 (3), 328-335, (July 1966).

2. Loo, S.G., "Spectral Properties and Optimum Reconstruction of Randomly Gated Stationary Random Signals", IEEE Trans. on Auto. Control , Oct. 1969, 564-567.

3. Papoulis, A., Signal Analysis, McGraw-Hill, NY, pp. 191-196 (1977).

4. Sankur, B., and Gerhardt, L.A., "Reconstruction of Signals from Nonuniform Samples", Conference Record of IEEE Int. Conf. on Communication, Seattle, Washington, (June 1973).

5. Shannon, C.E., "Communication in the Presence of Noise", Proc. IRE, 37, 10-21, (Jan. 1949).

6. Stearns, S.D., Digital Signal Analysis, Hayden Book Co., Rochelle Park, NJ (1975).

7. Whittaker, E.T., "On the Functions Which Are Represented By the Expansions of the Interpolation Theory", Proc. Roy. Soc. Edinburgh, 35, 181-194 (1915).

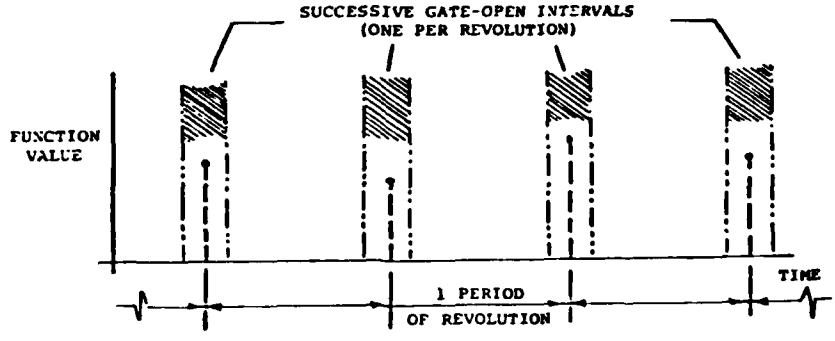

FIGURE A-1: Schematic of Gated LDA Measurements

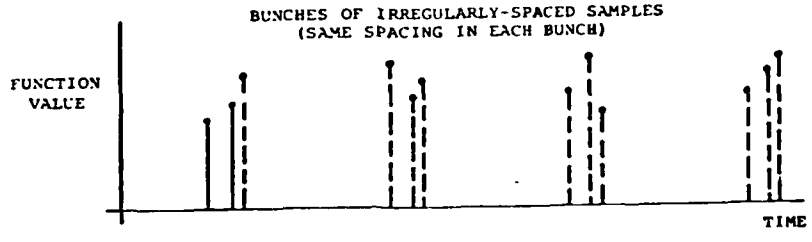

FIGURE A-2: Schematic of Papoulis' "Bunched" Samples

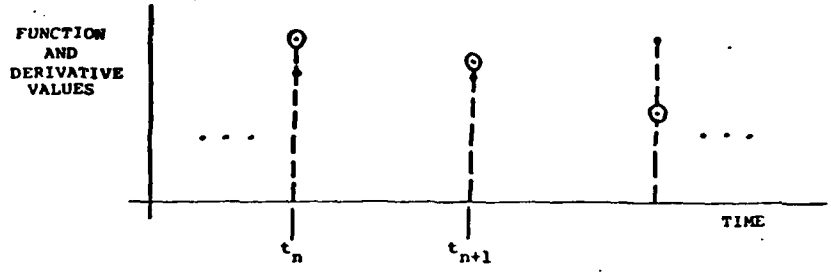

(a) Samples of Function Value and First Derivative at Evenly-Spaced Intervals

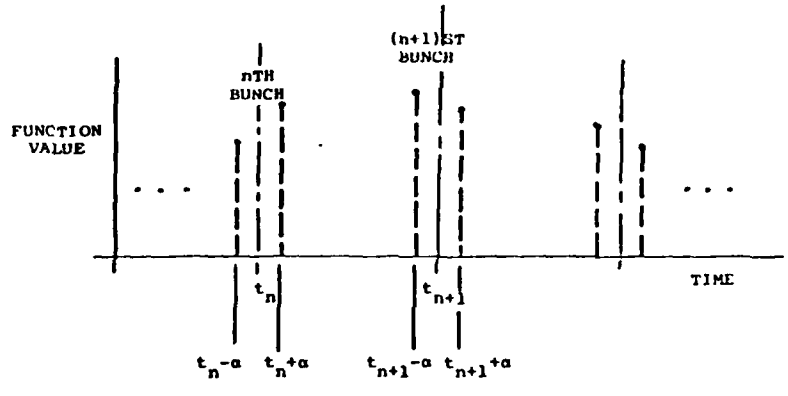

(b) Samples of Function Values in "Bunches" of Two

FIGURE A-3: Examples of Non-Conventional Sampling Schemes

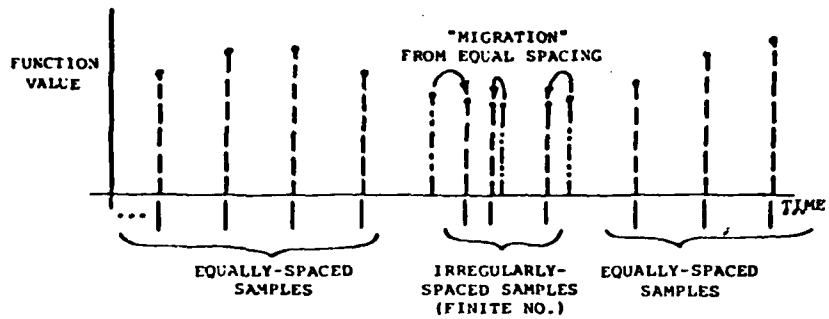

FIGURE A-4: Schematic of Yen's "Migrated" Samples

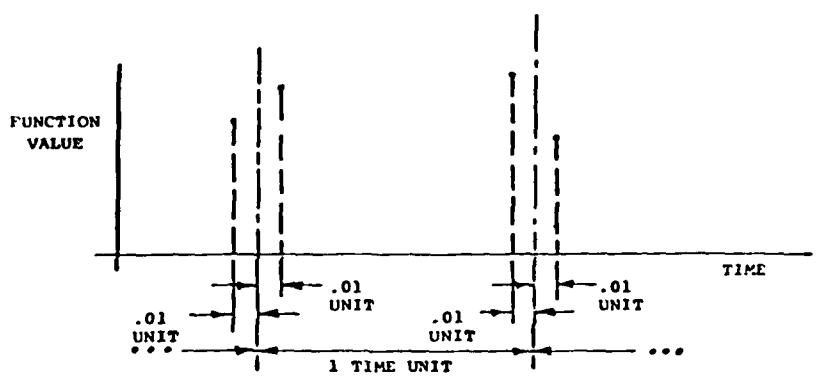

FIGURE A-5: Sampling Scheme for Simulations (Not to Scale)

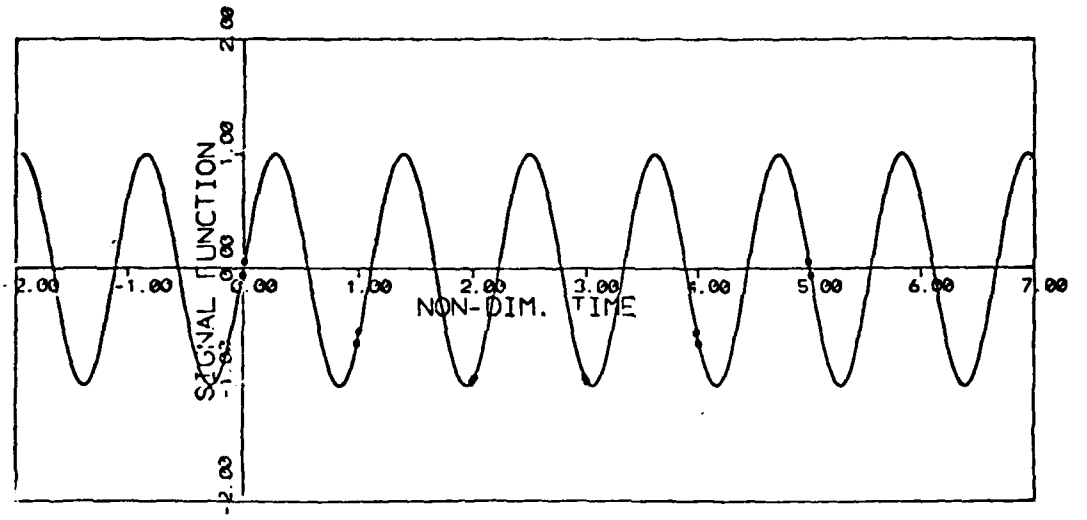

FIGURE A-6: Original (Sinusoidal) Signal Function Showing Bunched (Paired) Samples

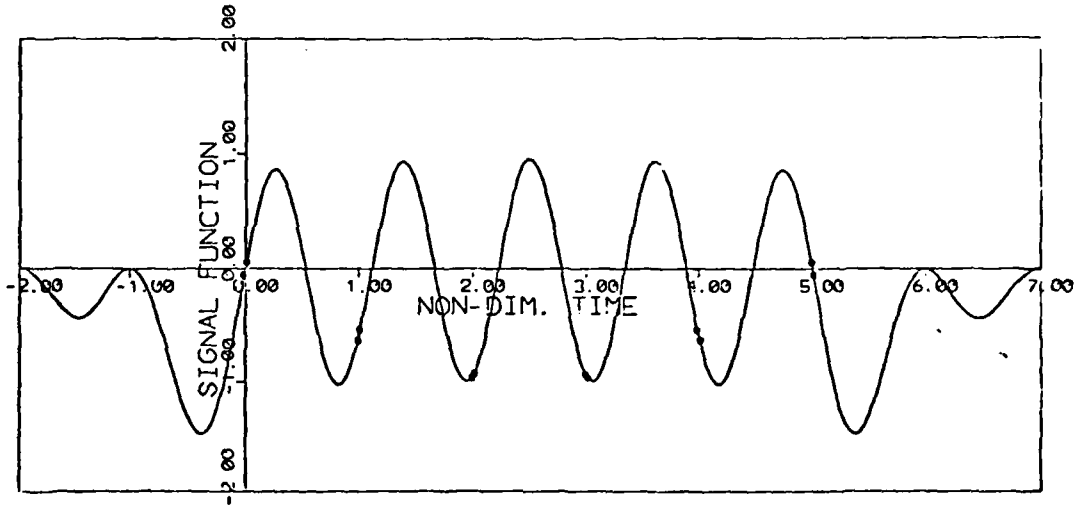

FIGURE A-7: Signal Reconstructed from Bunched Samples

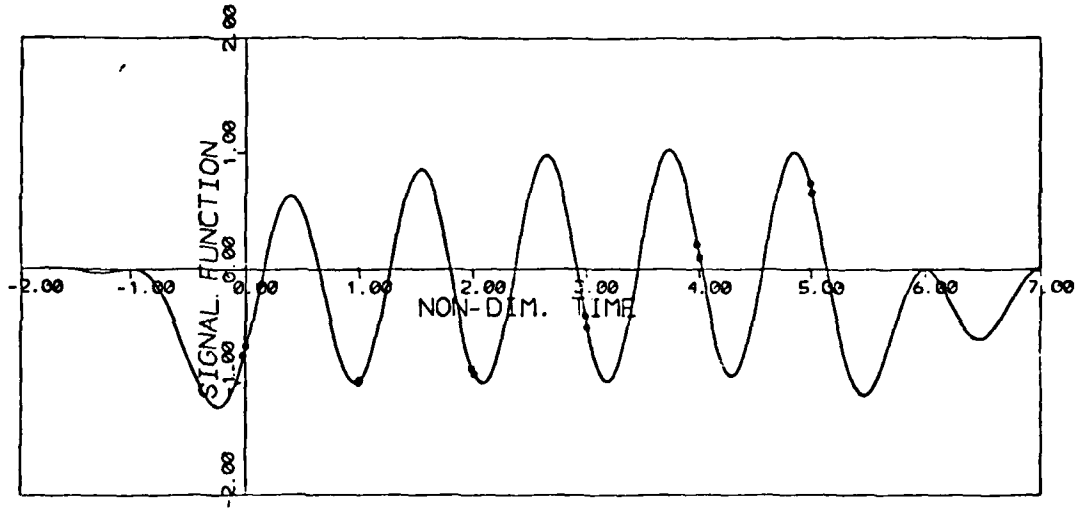

PHASE DIFFERENCE = 45°

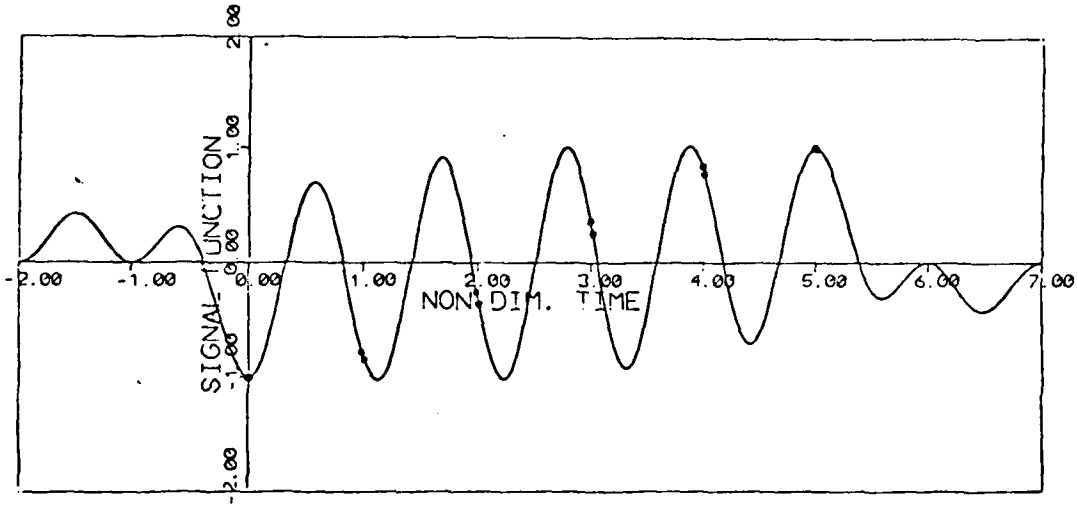

PHASE DIFFERENCE = 90°

FIGURE A-8: Signals Reconstructed for Various Relative Phases of Samples

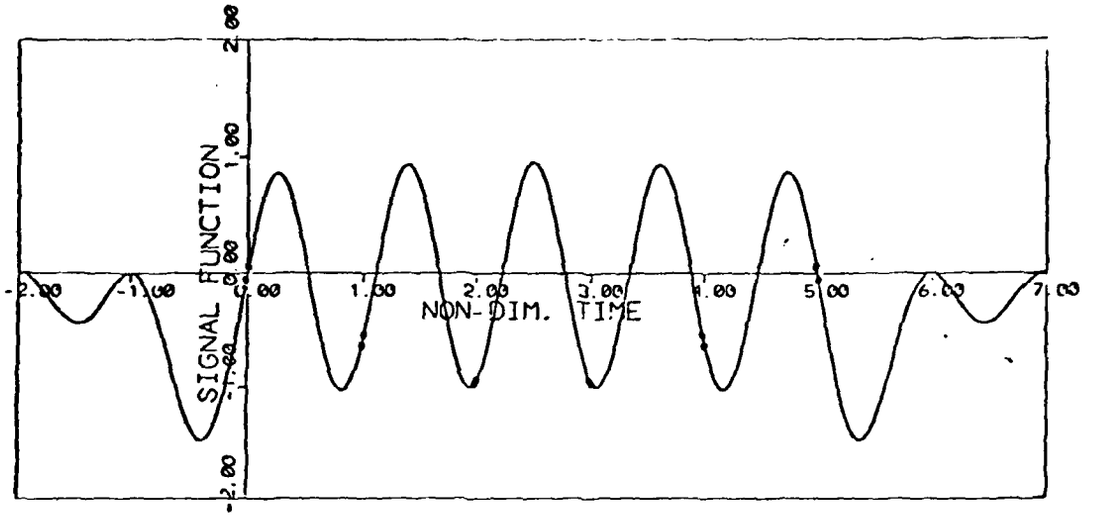

NON-DIM. FREQ. = 0.9

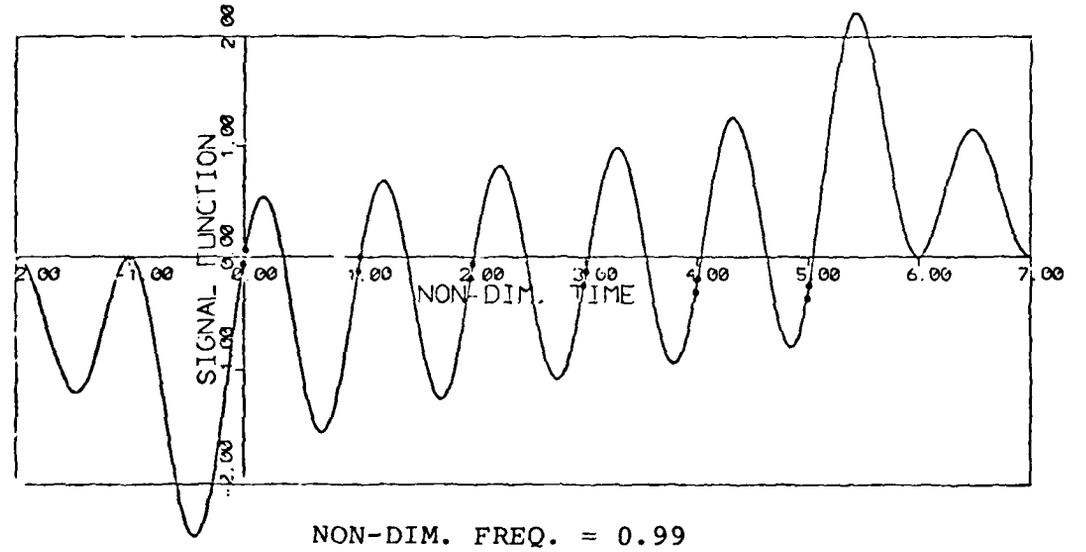

NON-DIM. FREQ. = 0.99

FIGURE A-9: Signal Reconstructions for Various Signal Frequencies

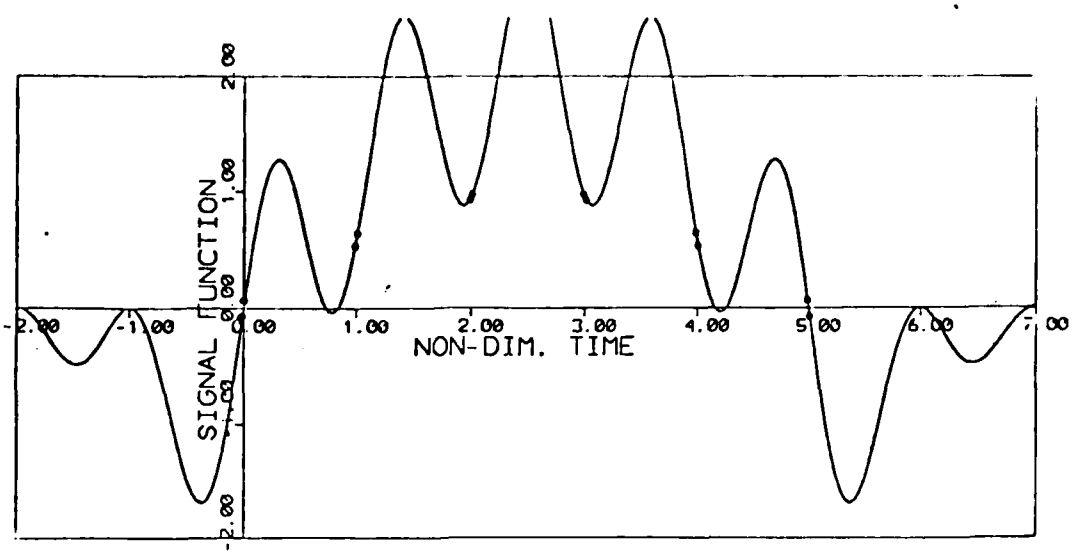

NON-DIM. FREQ. = 1.1

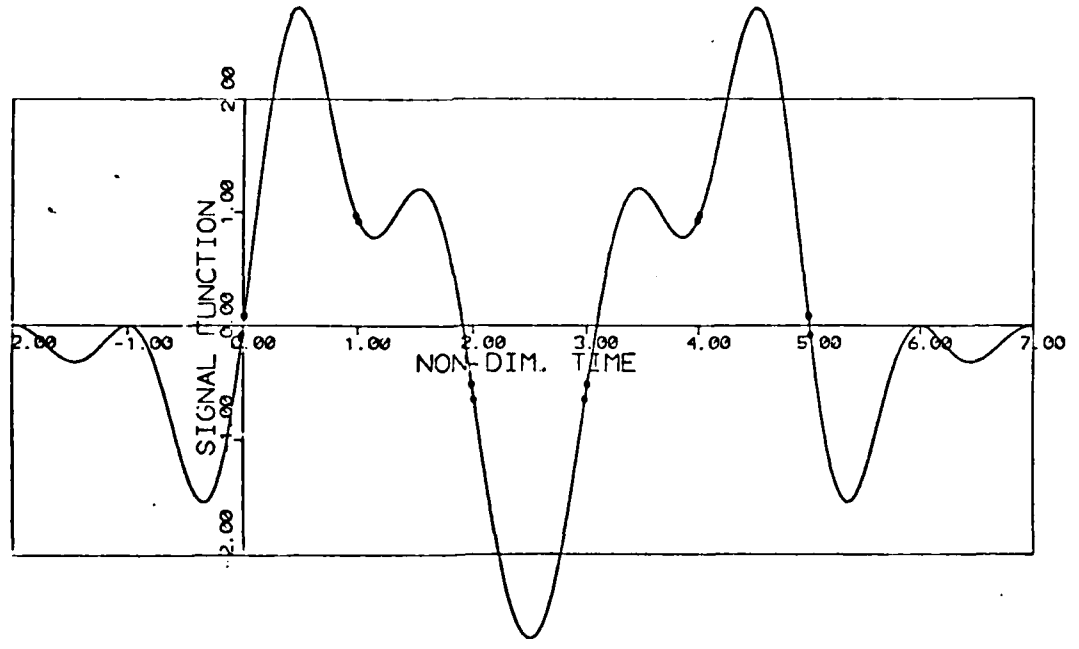

NON-DIM. FREQ. = 1.3

FIGURE A-9 (CONTINUED)

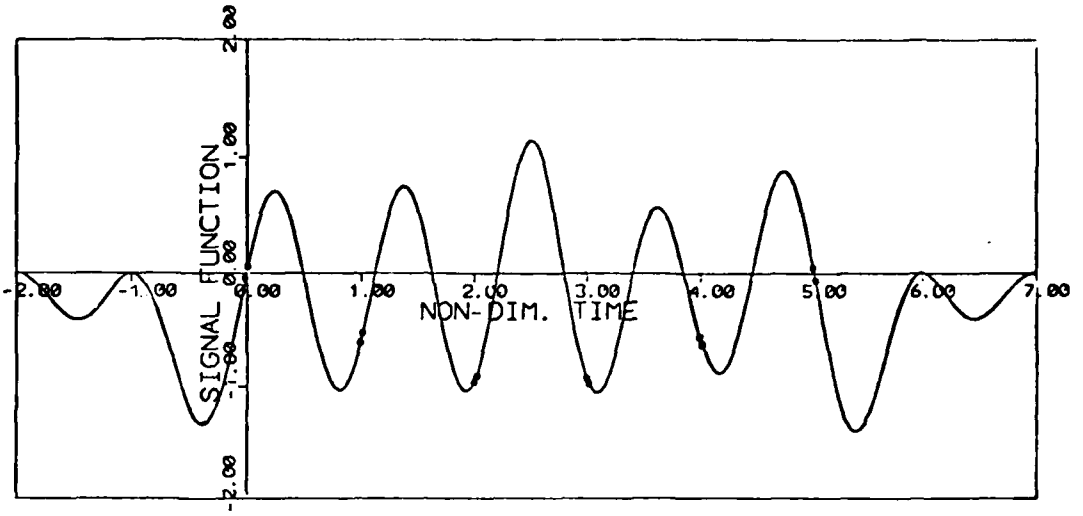

STD. DEV. OF ERROR = 0.01

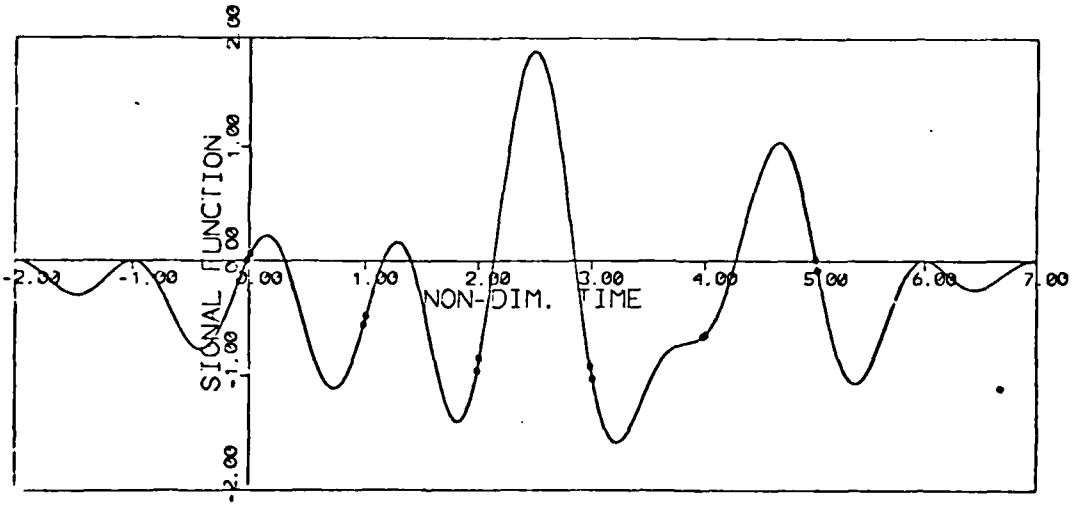

STD. DEV. OF ERROR = 0.05

FIGURE A-10: Signal Reconstructions for Various Experimental Errors

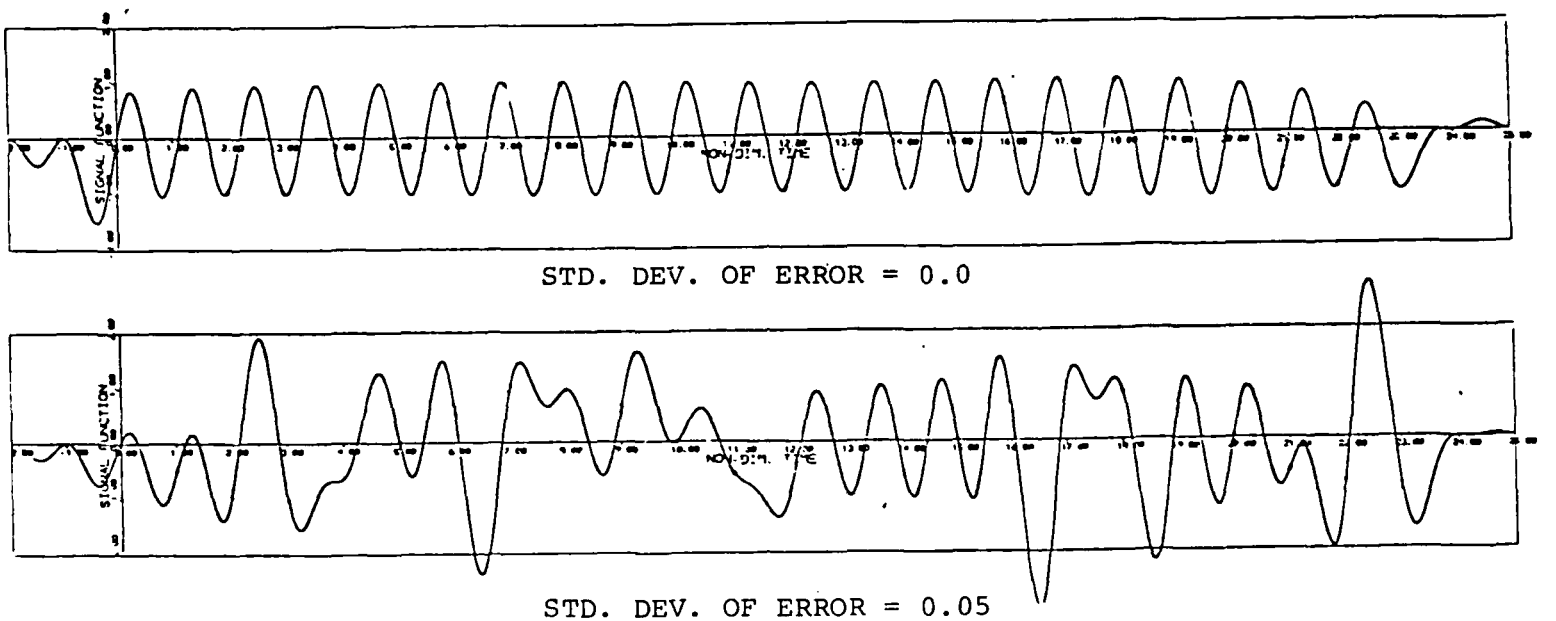

FIGURE A-11: Signal Reconstructions with Error and Increased Number of Samples (48)

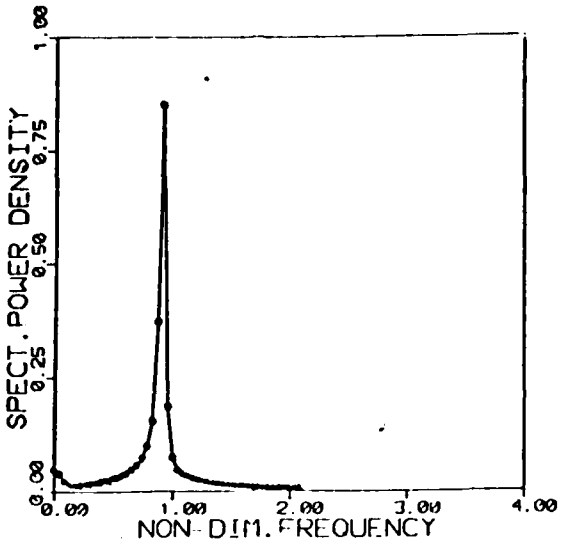

STD. DEV. OF ERROR = 0.0

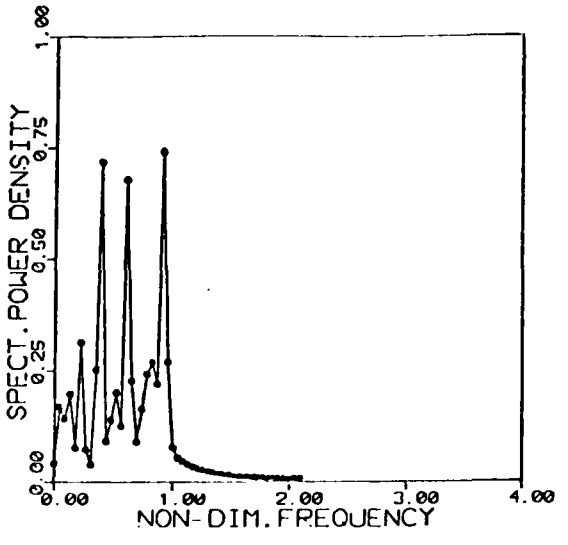

STD. DEV. OF ERROR = 0.05

FIGURE A-12: Spectra for Reconstructed Signals with Error and Increased Number of Samples (48)

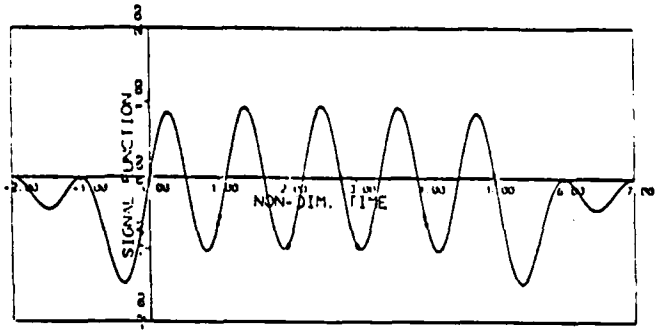

12 Samples

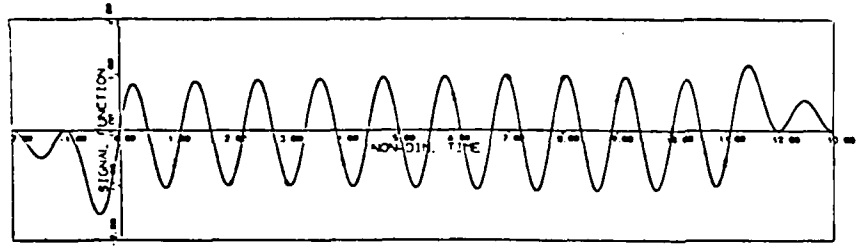

24 Samples

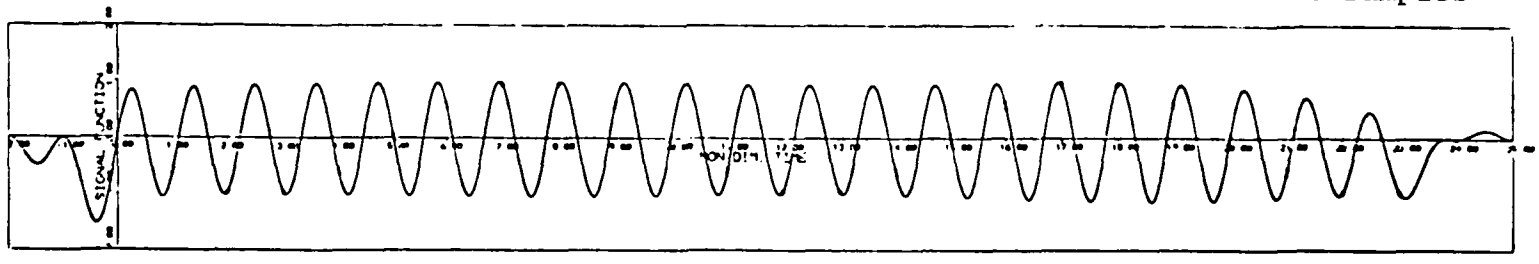

48 Samples

FIGURE A-13: Signal Reconstructions for Various Numbers of Samples (Various Overall Sampling Duration)

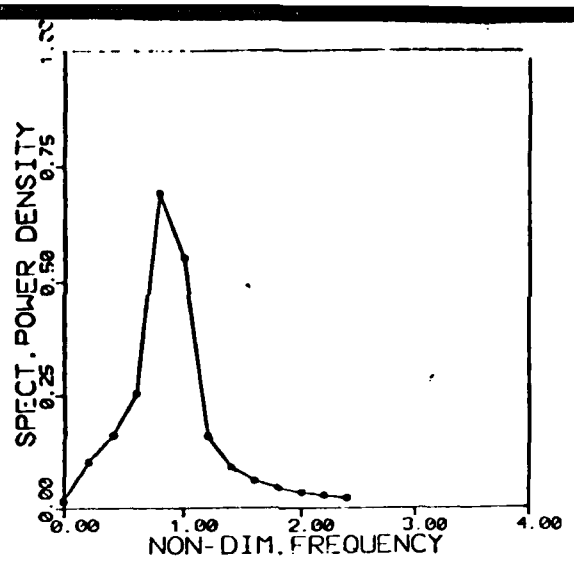

12 Samples

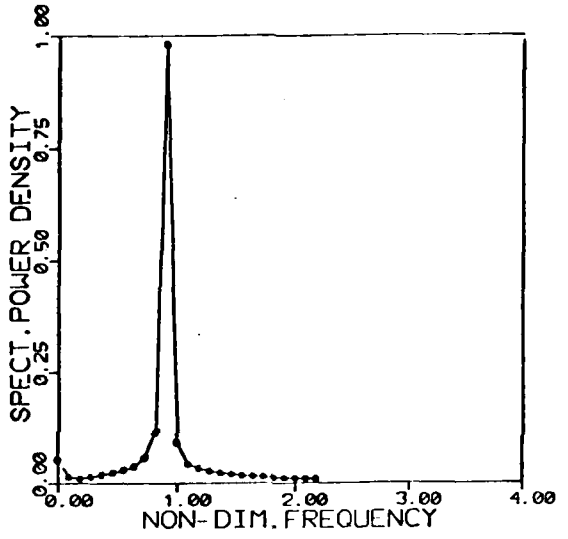

24 Samples

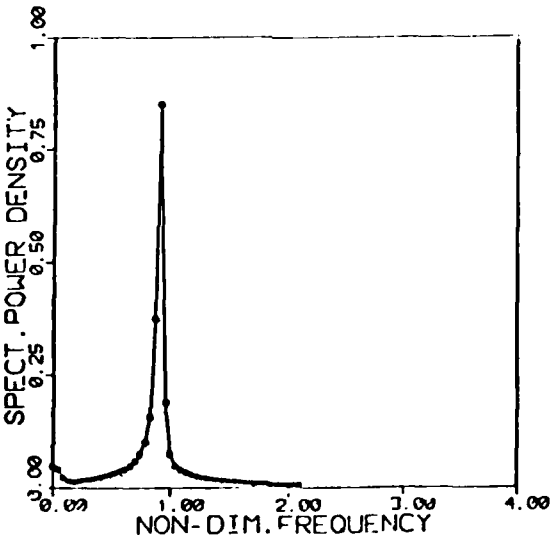

48 Samples

FIGURE A-14: Spectra of Reconstructed Signals For Various Numbers of Samples

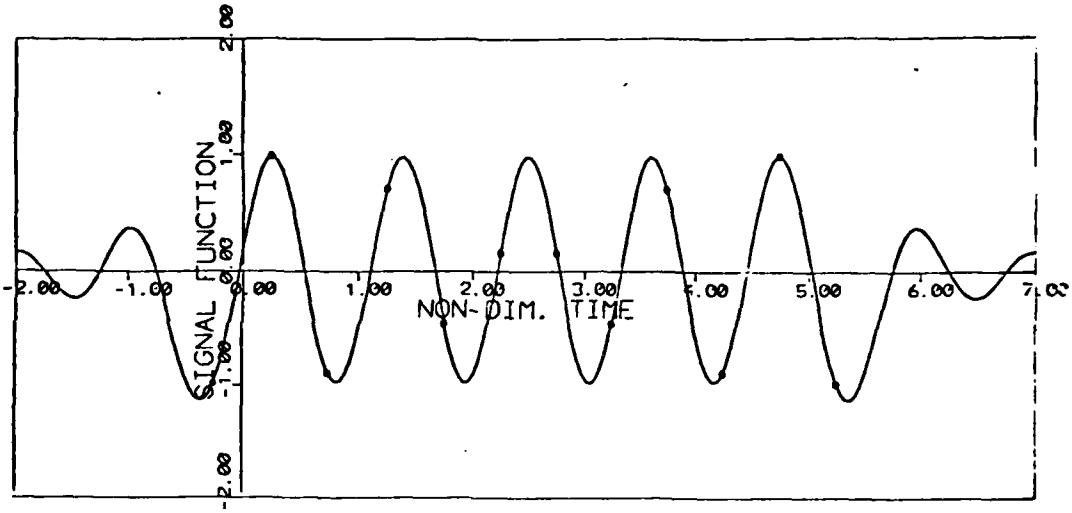

$\alpha = 0.25$

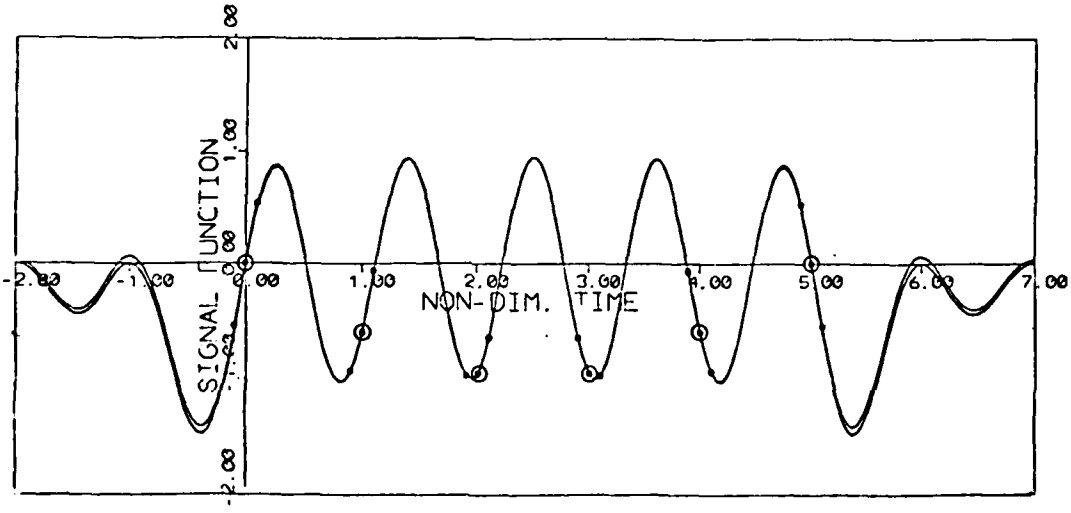

$\alpha = 0.10$ (·), $\alpha = 0.001$ (⊙ , 2 pts.)

FIGURE A-15: Signal Reconstructions for Various Gate-Open Intervals

(α = Non-Dim. Half Interval)

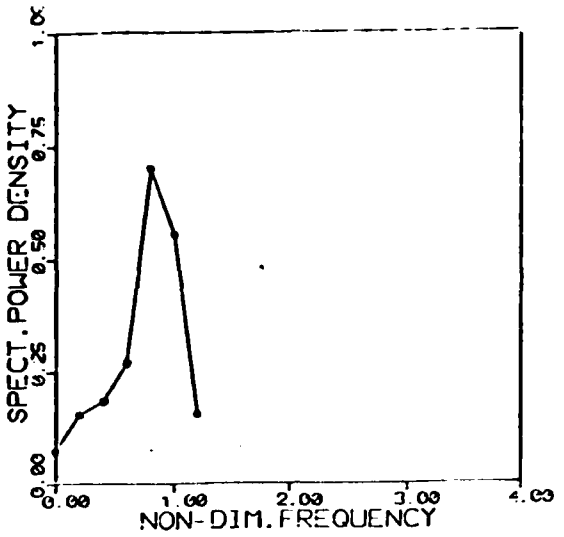

$\alpha = 0.25$

(Equally-Spaced Samples)

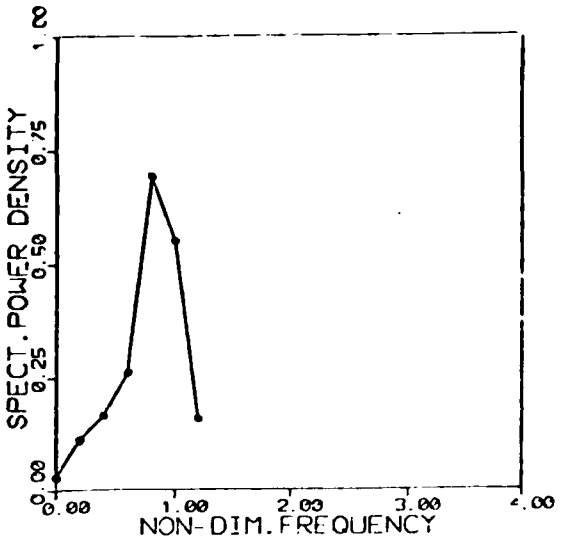

$\alpha = 0.10$

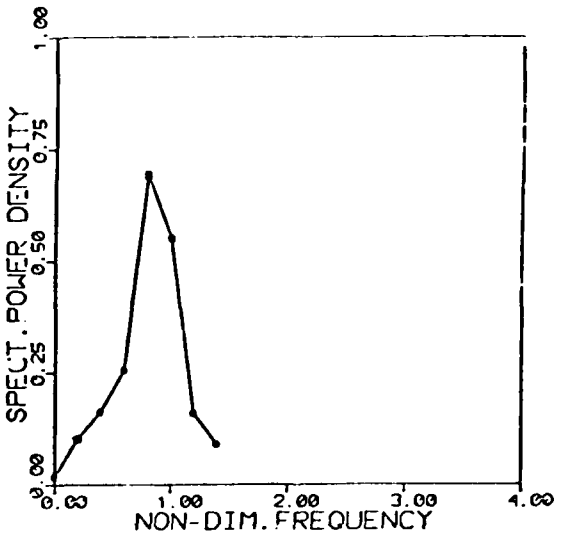

$\alpha = 0.001$

FIGURE A-16: Spectra of Reconstructed Signals For Various Gate-Open Intervals

(α = Non-Dim. Half Interval)

Appendix B

CASCADES OF NONUNIFORM LOADING

We wish to study initially steady nonuniform distributions of lift, or circulation, along cascades of airfoils. The simplest problem of this nature consists of an unstaggered infinite cascade of flat plate airfoils in two dimensional, incompressible flow. Consider the case where alternate blades of unit semichord have the same distribution of vorticity, and hence only two families of interdigitated blades may be distinguished. Referring to the sketch, the vertical velocities induced on the chordlines by this system may be shown to be given by

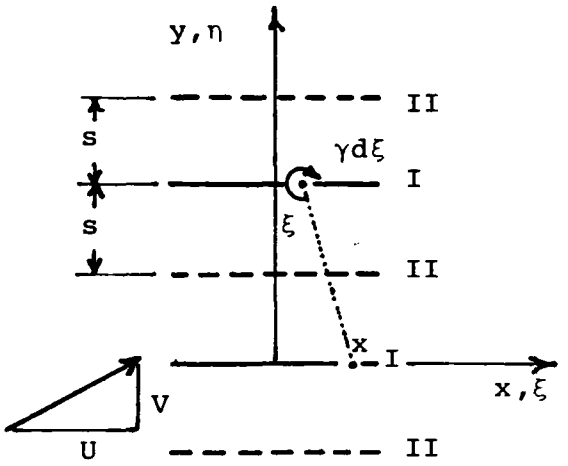

$$v_I(x) = \frac{1}{2\pi} \oint_{-1}^{1} K(\xi-x)\gamma_I(\xi)d\xi + \frac{1}{2\pi} \int_{-1}^{1} L(\xi-x)\gamma_{II}(\xi)d\xi \qquad (1)$$

$$v_{II}(x) = \frac{1}{2\pi} \oint_{-1}^{1} K(\xi-x)\gamma_{II}(\xi)d\xi + \frac{1}{2\pi} \int_{-1}^{1} L(\xi-x)\gamma_I(\xi)d\xi \qquad (2)$$

where

$$K(\xi-x) = \frac{\pi}{2s} \coth\left[\frac{\pi}{2s}(\xi-x)\right] \qquad (3)$$

$$L(\xi-x) = \frac{\pi}{2s} \tanh\left[\frac{\pi}{2s}(\xi-x)\right] \qquad (4)$$

It is the distributions γ_I and γ_{II} that are sought in this investigation. The kernels K and L are correct only for the present problem of an alternating distribution in passing from blade to blade; their derivation is perfectly straightforward. The largest magnitude

of the argument of the hyperbolic functions that can be expected is about 3 or 4, hence the kernels can be approximated quite accurately by

$$K(x-\xi) = (\xi-x)^{-1} + A_1(\xi-x) + A_2(\xi-x)^3 \qquad (3')$$

$$L(x-\xi) = \qquad B_1(\xi-x) + B_2(\xi-x)^3 \qquad (4')$$

where the constants A_1, A_2, B_1 and B_2 may be fitted by least squares over the interval $0< \xi-x <\pi(2s)^{-1}$. Note that the pitch/chord ratio is s/2.

To solve the coupled integral equations (1) and (2) it is convenient to transform the variables according to

$$\xi = \cos\theta \ , \quad x = \cos\phi \ , \quad 0 \leq \theta \text{ or } \phi \leq \pi \qquad (5)$$

In the arguments θ and ϕ the distributed circulations may be expanded in the so-called Glauert series

$$\gamma_I(\theta) = \tau_I \cot \tfrac{1}{2}\theta + \lambda_I \tan \tfrac{1}{2}\theta + \sum_1^\infty C_{In} \sin n\theta \qquad (6)$$

$$\gamma_{II}(\theta) = \tau_{II}\cot \tfrac{1}{2}\theta + \lambda_{II}\tan \tfrac{1}{2}\theta + \sum_1^\infty C_{IIn}\sin n\theta \qquad (7)$$

These distributions produce circulations round the representative airfoils equal to

$$\Gamma_{I,II} = \pi(\tau_{I,II} + \lambda_{I,II} + \tfrac{1}{2} C_{I1,III}) \qquad (8)$$

With these substitutions equations (1) and (2) may be transformed as follows

$$v_I(\phi) = \frac{1}{2\pi}\int_0^\pi [(\cos\theta - \cos\phi)^{-1} + A_1(\cos\theta - \cos\phi) + A_2(\cos\theta - \cos\phi)^3]$$
$$[\tau_I + \lambda_I + (\tau_I - \lambda_I)\cos\theta + \sum_1^\infty C_{In} \sin\theta \sin n\theta]d\theta$$
$$+ \frac{1}{2\pi}\int_0^\pi [B_1(\cos\theta - \cos\phi) + B_2(\cos\theta - \cos\phi)^3] \ .$$
$$[(\tau_{II} + \lambda_{II}) + (\tau_{II}-\lambda_{II})\cos\theta + \sum_1^\infty C_{IIn} \sin\theta \sin n\theta]d\theta \qquad (1')$$

$$v_{II}(\phi) = \frac{1}{2\pi} \oint_0^{\pi} [(\cos\theta - \cos\theta)^{-1} + A_1(\cos\theta - \cos\phi) + A_2(\cos\theta - \cos\phi)^3]$$

$$[\tau_{II} + \lambda_{II} + (\tau_{II} - \lambda_{II})\cos\theta + \sum_1^{\infty} C_{IIn} \sin\theta \sin n\theta]d\theta$$

$$+ \frac{1}{2\pi} \int_0^{\pi} [B_1(\cos\theta - \cos\phi) + B_2(\cos\theta - \cos\phi)^3]$$

$$[\tau_I + \lambda_I + (\tau_I - \lambda_I)\cos\theta + \sum_1^{\infty} C_{In} \sin\theta \sin n\theta]d\theta \qquad (2')$$

Using the well known singular integral

$$\int_0^{\pi} \frac{\cos n\theta}{\cos\theta - \cos\phi} d\theta = \pi \frac{\sin n\phi}{\sin\phi} \qquad (9)$$

the various trigonometric integrals may be evaluated with the following result.

$$2v_I(\phi) = (\tau_I - \lambda_I)(1 + \tfrac{1}{2} A_1 + \tfrac{9}{8} A_2) + C_{I2}(\tfrac{1}{4} A_1 + \tfrac{1}{2} A_2) + C_{I4}(\tfrac{1}{16} A_2)$$

$$+ (\tau_{II} - \lambda_{II})(\tfrac{1}{2} B_1 + \tfrac{9}{8} B_2) + C_{II2}(\tfrac{1}{4} B_1 + \tfrac{1}{2} B_2) + C_{II4}(\tfrac{1}{16} B_2)$$

$$+ \cos\phi[-C_{I1} - (\tau_I + \lambda_I + \tfrac{1}{2} C_{I1})A_1 + (-\tfrac{9}{4} \tau_I - \tfrac{9}{4} \lambda_I - \tfrac{3}{4} C_{I1} - \tfrac{3}{8} C_{I3})A_2]$$

$$+ \cos\phi[-(\tau_{II} + \lambda_{II} + \tfrac{1}{2} C_{II1})B_1 + (-\tfrac{9}{4} \tau_{II} - \tfrac{9}{4}\lambda_{II} - \tfrac{3}{4} C_{II1} - \tfrac{3}{8} C_{II3})B_2]$$

$$+ \cos 2\phi[-C_{I2} + (\tfrac{3}{4} \tau_I - \tfrac{3}{4} \lambda_I + \tfrac{3}{8} C_{I2})A_2] + \cos 2\phi[(\tfrac{3}{4}\tau_{II} - \tfrac{3}{4}\lambda_{II} + \tfrac{3}{8} C_{II2})B_2]$$

$$+ \cos 3\phi[-C_{I3} + (\tfrac{1}{4} \tau_I + \tfrac{1}{4} \lambda_I + \tfrac{1}{8} C_{I1})A_2] + \cos 3\phi[(\tfrac{1}{4}\tau_{II} + \tfrac{1}{4}\lambda_{II} + \tfrac{1}{8} C_{II1})B_2]$$

$$- \sum_4^{\infty} C_{In} \cos n\phi \quad . \qquad (10)$$

$$2v_{II}(\phi) = (\tau_{II} - \lambda_{II})(1 + \tfrac{1}{2} A_1 + \tfrac{9}{8} A_2) + C_{II2}(\tfrac{1}{4} A_1 + \tfrac{1}{2} A_2) + C_{II4}(\tfrac{1}{16} A_2),$$

etc. (11)

i.e. the subscripts I & II are interchanged throughout $2v_I$ to obtain $2v_{II}$.

The boundary condition on the flat plat airfoils requires that the induced velocities on the chordlines, v_I and v_{II}, be equal and opposite to the onset velocity component V of the mean flow, a constant. The expression of this B.C. leads to the matrix equation

$$[A]\ \{C\} = -2V\{10001000\} \tag{12}$$

where $\underline{C}$ is the vector of coefficients

$$\{C\} = \{\tau_I\ \lambda_I\ C_{I1}\ C_{I2}\ C_{I3}\ \tau_{II}\ \lambda_{II}\ C_{III}\ C_{II2}\ C_{II3}\} \tag{13}$$

and the 8 x 10 matrix $\underline{A}$ appears below

	τ_I	λ_I	C_{I1}	C_{I2}	C_{I3}	τ_{II}	λ_{II}	C_{III}	C_{II2}	C_{II3}
	$-a_{11}$	a_{11}	a_{12}	a_{13}	a_{14}	$-b_{11}$	b_{11}	b_{12}	b_{13}	b_{14}
0	$1+\frac{1}{2}A_1+\frac{9}{8}A_2$	$-1-\frac{1}{2}A_1-\frac{9}{8}A_2$	0	$\frac{1}{4}A_1+\frac{1}{2}A_2$	0	$\frac{1}{2}B_1+\frac{9}{8}B_2$	$-\frac{1}{2}B_1-\frac{9}{8}B_2$	0	$\frac{1}{4}B_1+\frac{1}{2}B_2$	0
	a_{21}	a_{21}	a_{22}	a_{23}	a_{24}	b_{21}	b_{21}	b_{22}	b_{23}	b_{24}
1	$-A_1-\frac{9}{4}A_2$	$-A_1-\frac{9}{4}A_2$	$-1-\frac{1}{2}A_1-\frac{3}{4}A_2$	0	$-\frac{3}{8}A_2$	$-B_1-\frac{9}{4}B_2$	$-B_1-\frac{9}{4}B_2$	$-\frac{1}{2}B_1-\frac{3}{4}B_2$	0	$-\frac{3}{8}B_2$
	$-a_{31}$	a_{31}	a_{32}	a_{33}	a_{34}	$-b_{31}$	b_{31}	b_{32}	b_{33}	b_{34}
2	$\frac{3}{4}A_2$	$-\frac{3}{4}A_2$	0	$-1+\frac{3}{8}A_2$	0	$\frac{3}{4}B_2$	$-\frac{3}{4}B_2$	0	$\frac{3}{8}B_2$	0
	a_{41}	a_{41}	a_{42}	a_{43}	a_{44}	b_{41}	b_{41}	b_{42}	b_{44}	b_{44}
3	$\frac{1}{4}A_2$	$\frac{1}{4}A_2$	$\frac{1}{8}A_2$	0	-1	$\frac{1}{4}B_2$	$\frac{1}{4}B_2$	$\frac{1}{8}B_2$	0	0
0	$\frac{1}{2}B_1+\frac{9}{8}B_2$	$-\frac{1}{2}B_1-\frac{9}{8}B_2$	0	$\frac{1}{4}B_1+\frac{1}{2}B_2$	0	$1+\frac{1}{2}A_1+\frac{9}{8}A_2$	$-1-\frac{1}{2}A_1-\frac{9}{8}A_2$	0	$\frac{1}{4}A_1+\frac{1}{2}A_2$	0
1	$-B_1-\frac{9}{4}B_2$	$-B_1-\frac{9}{4}B_2$	$-\frac{1}{2}B_1-\frac{3}{4}B_2$	0	$-\frac{3}{8}B_2$	$-A_1-\frac{9}{4}A_2$	$-A_1-\frac{9}{4}A_2$	$-1-\frac{1}{2}A_1-\frac{3}{4}A_2$	0	$-\frac{3}{8}A_2$
2	$\frac{3}{4}B_2$	$-\frac{3}{4}B_2$	0	$\frac{3}{8}B_2$	0	$\frac{3}{4}A_2$	$-\frac{3}{4}A_2$	0	$-1+\frac{3}{8}A_2$	0
3	$\frac{1}{4}B_2$	$\frac{1}{4}B_2$	$\frac{1}{8}B_2$	0	0	$\frac{1}{4}A_2$	$\frac{1}{4}A_2$	$\frac{1}{8}A_2$	0	-1

(14)

In terms of the 4x5 submatrices [a] and [b] it is clear that

$$[A] = \begin{bmatrix} a & b \\ b & a \end{bmatrix}$$

where the elements of [a] and [b] may be determined from [A]

The solution of these equations represents the possible configurations or distributions of circulation (bound vorticity) on the two families of airfoils constituting the cascade. To perform a systematic study of these solutions it is convenient to consider the four* cases delineated in the following table

Case	τ_I	λ_I	τ_{II}	λ_{II}
i	0		0	
ii	0			0
iii			0	0
iv		0		0

Afterwards a more general study may possibly be attempted.

Case (i) $[\tau_I = \tau_{II} = 0]$. This is the normal steady flow case, evidently stable in time and with the expected results: $\lambda_I = \lambda_{II}$, $C_{I1} = C_{III}$, etc. Both families of airfoils have identical distributions and hence the cascade loading is uniform in that sense. By making use of this demonstrable conclusion the equations may be simplified with the solution easily obtainable.

Upon deleting the 1st and 6th columns of matrix (14) and the 1st and 6th rows from the vector (13), it is found that equation (12) is separable into two equations that may be solved successively i.e., first for λ_I, λ_{II} .

$$\left[\begin{array}{cc:cc} a_{11} & a_{13} & b_{11} & b_{13} \\ a_{31} & a_{33} & b_{31} & b_{33} \\ \hdashline b_{11} & b_{13} & a_{11} & a_{13} \\ b_{31} & b_{33} & a_{31} & a_{33} \end{array}\right] \left[\begin{array}{c} \lambda_I \\ C_{I2} \\ \lambda_{II} \\ C_{II2} \end{array}\right] = -2V \left[\begin{array}{c} 1 \\ 0 \\ 1 \\ 0 \end{array}\right] \qquad (15)$$

*Two other cases may be discerned, but those cases merely interchange the roles of I & II.

$$\left[\begin{array}{cc:cc} a_{22} & a_{24} & b_{22} & b_{24} \\ a_{42} & a_{44} & b_{42} & b_{44} \\ \hdashline b_{22} & b_{24} & a_{22} & a_{24} \\ b_{42} & b_{44} & a_{42} & a_{44} \end{array}\right] \left[\begin{array}{c} C_{I1} \\ C_{I3} \\ C_{III} \\ C_{III} \end{array}\right] = -\lambda_I \left[\begin{array}{c} a_{21} \\ a_{41} \\ b_{21} \\ b_{41} \end{array}\right] - \lambda_{II} \left[\begin{array}{c} b_{21} \\ b_{41} \\ a_{21} \\ a_{41} \end{array}\right] - 2V \left[\begin{array}{c} 0 \\ 0 \\ 0 \\ 0 \end{array}\right] \qquad (16)$$

The symmetry displayed in the coefficient matrix of equation (15) results in $\lambda_I = \lambda_{II}$, $C_{I2} = C_{II2}$ and hence the equations may be reduced to

$$\left[\begin{array}{cc} a_{11} + b_{11} & a_{13} + b_{13} \\ a_{31} + b_{31} & a_{33} + b_{33} \end{array}\right] \left[\begin{array}{c} \lambda \\ C_2 \end{array}\right] = -2V \left[\begin{array}{c} 1 \\ 0 \end{array}\right] \qquad (15')$$

where $\lambda = \lambda_I$ or λ_{II} and $C_2 = C_{I2}$ or C_{II2}. The coefficient matrix in equation (16) may also be partitioned symmetrically into submatrices with the conclusion that $C_{I1} = C_{III}$, $C_{I3} = C_{II3}$ and hence

$$\left[\begin{array}{cc} a_{22} + b_{22} & a_{24} + b_{24} \\ a_{42} + b_{42} & a_{44} + b_{44} \end{array}\right] \left[\begin{array}{c} C_1 \\ C_3 \end{array}\right] = -\lambda \left[\begin{array}{c} a_{21} + b_{21} \\ a_{41} + b_{41} \end{array}\right] \qquad (16')$$

where $C_1 = C_{I1}$ or C_{III} and $C_3 = C_{I3}$ or C_{II3} .

A rougher approximation may be obtained by letting $A_2 = B_2 = 0$ in which case it is found that $C_{I2} = C_{II2} = C_{I3} = C_{II3} = 0$ and

$$\lambda_I = \lambda_{II} = \frac{2V}{1+\frac{1}{2}A_1+\frac{1}{2}B_1}, \quad C_{I1} = C_{III} = -\lambda \frac{A_1 + B_1}{1+\frac{1}{2}A_1+\frac{1}{2}B_1}$$

Finally, to recover the familiar isolated airfoil result it is only necessary to let $A_1 = B_1 = 0$ and so arrive at

$$\lambda_{is} = 2V, \quad C = 0.$$

The role of U, a measure of the massflow or throughput, determines the incidence for specified V, and hence the cascade loading, flow deflection, etc. In order to explore the local flow magnitudes, stagnation points and possible flow reversals it is interesting to take a short digression and consider the flow pattern associated with a column of point vortices of strength $\Gamma = \pi(\lambda + \frac{1}{2}C_1)$.

Column of Vortices

Each airfoil has a circulation whose strength may be expressed as $\Gamma = \pi(\lambda + \frac{1}{2}C_1) = 2\pi VK$, where λ and C_1 in turn are proportional to V so that

$$K = \frac{1}{2} \frac{\lambda(V) + \frac{1}{2}C_1(V)}{V} \tag{8i}$$

A vertical row of stationary vortices of strength $\Gamma = 2\pi VK$ and spacing s immersed in an onset flow with components U, V has a complex potential ($z = x + iy$)

$$F = \phi + i\psi = (U - iV)z + iVK \log \sinh \frac{\pi z}{s} \tag{19}$$

The corresponding stream function is

$$\psi = Uy - V[x - \tfrac{1}{2}K \log(\sinh^2 \frac{\pi x}{s} + \sin^2 \frac{\pi y}{s})] \tag{20}$$

and the complex velocity is

$$u - iv = U - iV + \frac{i\pi VK}{s} \coth \frac{\pi z}{s} \tag{21}$$

Extracting the u,v components results in

$$u = U + \frac{\pi}{s} VK \frac{\sin(2\pi y/s)}{\cosh(2\pi x/s) - \cos(2\pi y/s)} \tag{22}$$

and

$$v = V - \frac{\pi}{s} VK \frac{\sinh(2\pi x/s)}{\cosh(2\pi x/s) - \cos(2\pi y/s)}$$

Analysis of Eq. (22) shows that a reverse flow region may exist on the intervals $n - \frac{1}{2} < y/s < n$ for any integer n and for x near zero. This reversal region is enlarged for small values of U relative to V, i.e. for large incidence. As such it may be thought of as a "stall" zone, although it occurs near the nose on the pressure side of the airfoils which are modelled by the row of discrete lifting vortices. Consequently, this type of reverse flow should be associated with "cascade stall". The nonoccurrence of such reverse flow patches may be explained by stability considerations which dictate a shift to another flow pattern as the incidence is progressively increased.

Column of Countervortices

A second digression is instructive at this point. A column of equispaced vortices of constant strength $\Gamma = 2\pi VK$ but of alternating sign is the simplest analog of case (ii) to follow.

The complex potential for this case is

$$F = \phi + i\psi = (U - iV)z + iVK \log \tanh \frac{\pi z}{2s} \tag{23}$$

with corresponding stream function

$$\psi = Uy - V\left[x - \frac{1}{2}K \log \frac{\cosh \frac{\pi x}{s} + \cos \frac{\pi y}{s}}{\cosh \frac{\pi x}{s} - \cos \frac{\pi y}{s}}\right] \tag{24}$$

*

The u,v components of velocity for this flow are

$$u = U + \pi \frac{VK}{s} \frac{\sin \pi y/s \cosh \pi x/s}{\cosh^2 \pi x/s - \cos^2 \pi y/s} \tag{25}$$

and

$$v = V - \pi \frac{VK}{s} \frac{\cos \pi y/s \sinh \pi x/s}{\cosh^2 \pi x/s - \cos^2 \pi y/s} \tag{26}$$

*It is instructive to trace the streamlines $\psi=0$, $\psi=Us$, $\psi=2Us$, $\psi=3Us$.

This gives, near x=0, a sequence of horizontal "jets", alternating between right- and left-flowing and with v-components to satisfy continuity. The velocity U biases these jets to have larger core velocities in the right-flowing "jets". The perturbations die out with $|x| > 0$.

Case (ii) [$\tau_I=0$, $\lambda_{II}=0$]. This requirement of a Kutta condition (smooth flow) at the leading edge of family - II airfoils should provide additional insight concerning reversed flows. Displaying the matrices that obtain for this case

$$\begin{bmatrix} a_{11} & a_{13} & -b_{11} & b_{13} \\ a_{31} & a_{33} & -b_{31} & b_{33} \\ b_{11} & b_{13} & -a_{11} & a_{13} \\ b_{31} & b_{33} & -a_{31} & a_{33} \end{bmatrix} \begin{bmatrix} \lambda_I \\ C_{I2} \\ \tau_{II} \\ C_{II2} \end{bmatrix} = -2V \begin{bmatrix} 1 \\ 0 \\ 1 \\ 0 \end{bmatrix} \tag{27}$$

$$\left[\begin{array}{cc:cc} a_{22} & a_{24} & b_{22} & b_{24} \\ a_{42} & a_{44} & b_{42} & b_{44} \\ \hdashline b_{22} & b_{24} & a_{22} & a_{24} \\ b_{42} & b_{44} & a_{42} & a_{44} \end{array}\right] \begin{bmatrix} C_{I1} \\ C_{I3} \\ C_{II1} \\ C_{II3} \end{bmatrix} = -\lambda_I \begin{bmatrix} a_{21} \\ a_{41} \\ b_{21} \\ b_{41} \end{bmatrix} - \tau_{II} \begin{bmatrix} b_{21} \\ b_{41} \\ a_{21} \\ a_{41} \end{bmatrix} - 2V \begin{bmatrix} 0 \\ 0 \\ 0 \\ 0 \end{bmatrix} \tag{28}$$

Comparing equations (17) and (15) it is clear that the sign changes in the third column imply in case (ii)

$$-\tau_{II} = \lambda_I, \quad C_{I2} = C_{II2} \tag{29}$$

and equation (15') (in which λ is identified with λ_I) may be employed to find these values.

The symmetry conditions applied to equation (18) result in

$$C_{I1} = -C_{II1}, \quad C_{I3} = -C_{II3} \tag{30}$$

and

$$\begin{bmatrix} a_{22} - b_{22} & a_{24} - b_{24} \\ a_{42} - b_{42} & a_{44} - b_{44} \end{bmatrix} \begin{bmatrix} C_{I1} \\ C_{I3} \end{bmatrix} = - \lambda_I \begin{bmatrix} a_{21} - b_{21} \\ a_{41} - b_{41} \end{bmatrix} \tag{31}$$

The most interesting conclusion of studying case (ii) is the fact that τ_{II} is negative, presuming λ_I is positive. This means that there is flow rearward along the pressure surface of the family-II profiles near the trailing edge. Questions of separation at the sharp trailing edge are ignored for the time being. The flow then turns around the TE and flows forward (upstream in the sense of the mean flow) along the suction surface. Since $\lambda_I = -\tau_{II}$, $C_{I1} = -C_{III}$ and $\lambda_{II} = \tau_I = 0$, the circulation alternates between $\pm \pi(\lambda_I + \frac{1}{2} C_{I1})$ from blade to blade; there is no net deflection of the throughflow far from the cascade. This could be used as a definition of "cascade stall".

Case (iii) [$\tau_{II}=0$, $\lambda_{II}=0$]. There is no solution because $\underline{C}$ is singular for this case. Physically this corresponds to the fact that "shock-free"* flow cannot be obtained with an unstaggered cascade of uncambered airfoils, except at the unloaded (zero deflection) condition. Evidently this restriction carries over to nonuniform cascade flow when only alternate blades are supposed to be shock-free.

Case (iv) [$\lambda_I = \lambda_{II}=0$]. The solution for this case may be deduced by considering a reflection of case (i). Thus $\tau_I = \tau_{II}$ = negative number is an immediate conclusion. Comparison with equations (15) and (15') leads to the solution

$$\begin{bmatrix} a_{11} + b_{11} & a_{13} + b_{13} \\ a_{31} + b_{31} & a_{33} + b_{33} \end{bmatrix} \begin{bmatrix} -\tau \\ C_2 \end{bmatrix} = -2V \begin{bmatrix} 1 \\ 0 \end{bmatrix} \tag{32}$$

* local incidence equals zero at the leading edge.

and similarly, a study of equations (16) and (16') leads to the conclusion

$$\begin{bmatrix} a_{22} + b_{22} & a_{23} + b_{24} \\ a_{42} + b_{42} & a_{44} + b_{44} \end{bmatrix} \begin{bmatrix} C_1 \\ C_3 \end{bmatrix} = -\tau \begin{bmatrix} a_{21} + b_{21} \\ a_{41} + b_{41} \end{bmatrix} \tag{33}$$

where $\tau = \tau_I$ or τ_{II}, $C_1 = C_{I1}$ or C_{III}, etc.

Since the circulation around each airfoil is now (case (iv))

$$\Gamma = \pi(\tau + \tfrac{1}{2} C_1) \tag{34}$$

and this is a negative number, the airfoils of case (iv) produce a negative deflection of the flow; the mean flow is accelerated in passing through the cascade.

Conclusions

Cases (i)(ii) and (iv) taken together present three regimes of cascade flow having positive, zero and "negative" flow deflection. When the horizontal component of mean velocity U is considered. Case (i) corresponds to normal flow from left to right at low incidence; case (ii) is a kind of "cascade stall" in which the deflection drops to zero and case (iv) is best interpreted as reverse flow with uniform loading along the cascade. Plotting upstream and downstream flow angles α_1 & α_2 as a function of V/U as in the sketch, illustrates this behavior (unit solidity assumed).

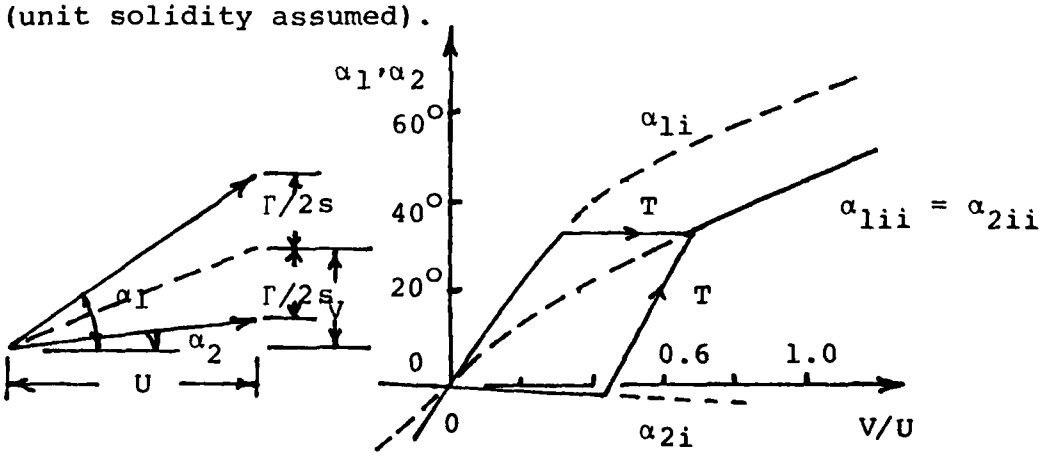

The transition from type (i) to type (ii) characteristics is unknown. In fact stability considerations must be invoked with the likely result that case (ii) is not an attainable steady state configuration. A purely hypothetical transition is shown by the solid lines in the sketch.

Stability

In order to study stability one must allow for time dependency by allowing the λ, τ and C coefficients to vary with time, and also accounting for the shed vorticity as the circulations Γ_I, Γ_{II} change with the evolution of time. This analysis will be attempted and reported in a future report.

Example

A numerical example was pursued for the following parameter values:

$$s = 2 \text{ (i.e. } s/c = 1) \qquad \Gamma = 2\pi VK = \pi(\lambda + \tfrac{1}{2} C_1) \qquad K = \frac{\lambda + \frac{1}{2} C_1}{2V}$$

$$A_1 = \frac{\pi}{2s} \; \frac{1}{3} \; \frac{\pi}{2s} = .205617$$

$$A_2 = \frac{\pi}{2s} \left(-\frac{1}{45}\right) \left(\frac{\pi}{2s}\right)^3 = -.008456$$

$$B_1 = \frac{\pi}{2s} \; \frac{\pi}{2s} = .616850$$

$$B_2 = \frac{\pi}{2s} \left(-\frac{1}{3}\right) \left(\frac{\pi}{2s}\right)^3 = -.126835$$

$$a_{11} = -1 - \tfrac{1}{2}A_1 - \tfrac{9}{8}A_2 = -1.093296 \qquad b_{11} = -\tfrac{1}{2}B_1 - \tfrac{9}{8}B_2 = -0.165736$$

$$a_{21} = -A_1 - \tfrac{9}{4}A_2 = -0.186591 \qquad b_{21} = -B_1 - \tfrac{9}{4}B_2 = -0.331471$$

$$a_{31} = -\tfrac{3}{4}A_2 = 0.006342 \qquad b_{31} = -\tfrac{3}{4}B_2 = 0.095126$$

$$a_{41} = \tfrac{1}{4}A_2 = -.002114 \qquad b_{41} = \tfrac{1}{4}B_2 = -0.031709$$

(continued)

$$a_{22} = -1-\tfrac{1}{2}A_1-\tfrac{3}{4}A_2 = -1.096467 \qquad b_{22} = -\tfrac{1}{2}B_1-\tfrac{3}{4}B_2 = -0.213299$$

$$a_{42} = \tfrac{1}{8}A_2 = -0.001057 \qquad b_{42} = \tfrac{1}{8}B_2 = -0.015854$$

$$a_{13} = \tfrac{1}{4}A_1+\tfrac{1}{2}A_2 = 0.047176 \qquad b_{13} = \tfrac{1}{4}B_1+\tfrac{1}{2}B_2 = 0.090795$$

$$a_{33} = -1+\tfrac{3}{8}A_2 = -1.003171 \qquad b_{33} = \tfrac{3}{8}B_2 = -0.047563$$

$$a_{24} = -\tfrac{3}{8}A_2 = 0.003171 \qquad b_{24} = -\tfrac{3}{8}B_2 = 0.047563$$

$$a_{44} = -1 = -1.000000$$

CASE (i)

[A]

$$\begin{bmatrix}
-1.093296 & 0 & 0.047176 & 0 & -0.165736 & 0 & 0.090795 & 0 \\
-0.186591 & -1.096467 & 0 & 0.003171 & -0.331471 & -0.213299 & 0 & 0.047563 \\
0.006342 & 0 & -1.003171 & 0 & 0.095126 & 0 & -0.047563 & 0 \\
-0.002114 & -0.001057 & 0 & -1 & -0.031709 & -0.015854 & 0 & 0 \\
-0.165736 & 0 & 0.090795 & 0 & -1.093296 & 0 & 0.047176 & 0 \\
-0.331471 & -0.213299 & 0 & 0.047563 & -0.186591 & -1.096467 & 0 & 0.003171 \\
0.095126 & 0 & -0.047563 & 0 & 0.006342 & 0 & -1.003171 & 0 \\
-0.031709 & -0.015854 & 0 & 0 & -0.002114 & -0.001057 & 0 & -1
\end{bmatrix}
\qquad
\frac{1}{V}\{C\}
\begin{bmatrix}
1.605512 \\ -0.636727 \\ 0.155042 \\ -0.043536 \\ 1.605512 \\ -.636727 \\ 0.155042 \\ -0.043536
\end{bmatrix}$$

Det = 1.338054007

$\Gamma = \pi[1.605512 - \tfrac{1}{2}(.636727)]V = 4.044V$

$$\left.\frac{\Gamma}{2s}\right|_{s=2} = 1.011V$$

CASE (ii)

[A]

								$\frac{1}{V}\{C\}$
a_{11}	a_{12}	a_{13}	a_{14}	$-b_{11}$	b_{12}	b_{13}	b_{14}	
-1.093296	0	0.047176	0	0.165736	0	0.090795	0	1.60551
a_{21}	a_{22}	a_{23}	a_{24}	b_{21}	b_{22}	b_{23}	b_{24}	
-0.186591	-1.096467	0	0.003171	-0.331471	-0.213299	0	0.047563	0.26079
a_{31}	a_{32}	a_{33}	a_{34}	$-b_{31}$	b_{32}	b_{33}	b_{34}	
0.006342	0	-1.003171	0	-0.095126	0	-0.047563	0	0.15504
a_{41}	a_{42}	a_{43}	a_{44}	b_{41}	b_{42}	b_{43}	b_{44}	
-0.002114	-0.001057	0	-1	-0.031709	-0.015854	0	0	0.051373
b_{11}	b_{12}	b_{13}	b_{14}	$-a_{11}$	a_{12}	a_{13}	a_{14}	
-0.165736	0	0.090795	0	1.093296	0	0.047176	0	-1.60551
b_{21}	b_{22}	b_{23}	b_{24}	a_{21}	a_{22}	a_{23}	a_{24}	
-0.331471	-0.213299	0	0.047563	-0.186591	-1.096467	0	0.003171	-0.260795
b_{31}	b_{32}	b_{33}	b_{34}	$-a_{31}$	a_{32}	a_{33}	a_{34}	
0.095126	0	-0.047563	0	-0.006342	0	-1.003171	0	0.155042
b_{41}	b_{42}	b_{43}	b_{44}	a_{41}	a_{42}	a_{43}	a_{44}	
-0.031709	-0.015854	0	0	-0.002114	-0.001057	0	-1	-0.051374

Det = -1.338054

$\Gamma_I = \pi\ [1.605512 + \frac{1}{2}(0.260795)] = 5.453521$

$\Gamma_{II} = \pi\ [-1.605512 - \frac{1}{2}(0.260795)] = -5.453521$

$$\left.\frac{\Gamma}{2s}\right|_{avg} = 0$$

CASE (iii)

[A]

$$\begin{bmatrix}
1.093296 & -1.093296 & 0 & 0.047176 & 0 & 0 & 0.090795 & 0 \\
-0.186591 & -0.186591 & -1.096467 & 0 & 0.003171 & -0.213299 & 0 & 0.047563 \\
-0.006342 & 0.006342 & 0 & -1.003171 & 0 & 0 & -0.047563 & 0 \\
-0.002114 & -0.002114 & -0.001057 & 0 & -1 & -0.015844 & 0 & 0 \\
0.165736 & -0.165736 & 0 & 0.090795 & 0 & 0 & 0.047176 & 0 \\
-0.331471 & -0.331471 & 0.213299 & 0 & 0.047563 & -1.096467 & 0 & 0.003171 \\
-0.095126 & 0.095126 & 0 & -0.047563 & 0 & 0 & -1.003171 & 0 \\
-0.031709 & -0.031709 & -0.015854 & 0 & 0 & -0.001057 & 0 & -1
\end{bmatrix}$$

{C}

$$\begin{bmatrix}
\tau_I \\ \lambda_I \\ C_{I1} \\ C_{I2} \\ C_{I3} \\ C_{II1} \\ C_{II2} \\ C_{II3}
\end{bmatrix}$$

Det = 1.256725×10^{-13} Singular

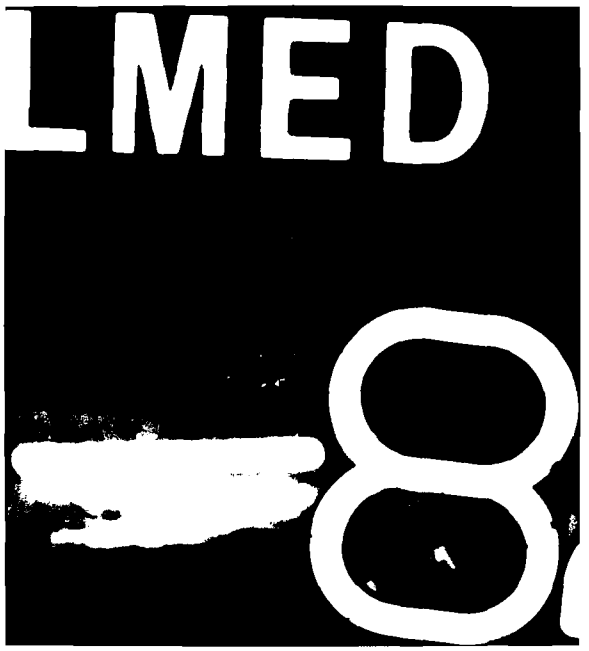
LMED
8